Miocene magmatism and tectonics of the easternmost sector of the Calama–Olacapato–El Toro fault system in Central Andes at ~24°S: Insights into the evolution of the Eastern Cordillera

R. Mazzuoli[†]
Dipartimento di Scienze della Terra, Università di Pisa, Pisa, Italy

L. Vezzoli
Dipartimento di Scienze Chimiche e Ambientali, Università degli Studi dell'Insubria, Como, Italy

R. Omarini
Facultad de Ciencias Naturales, Universidad Nacional de Salta, CONICET, Argentina

V. Acocella
Dipartimento di Scienze Geologiche, Università Roma Tre, Roma, Italy

A. Gioncada
Dipartimento di Scienze della Terra, Università di Pisa, Pisa, Italy

M. Matteini
CNPq, Institute of Geosciences, University of Brasilia, Brasilia, Brazil

A. Dini
Istituto di Geoscienze e Georisorse, CNR, Pisa, Italy

H. Guillou
Laboratoire des Sciences du Climat et de l'Environnement CNRS, Gif-sur-Yvette, France

N. Hauser
Facultad de Ciencias Naturales, Universidad Nacional de Salta, CONICET, Argentina

A. Uttini
Dipartimento di Scienze Chimiche e Ambientali, Università degli Studi dell'Insubria, Como, Italy

S. Scaillet
Laboratoire des Sciences du Climat et de l'Environnement CNRS, Gif-sur-Yvette, France

ABSTRACT

The Miocene Las Burras–Almagro–El Toro magmatic complex lies ~300 km to the east of the Central Andes volcanic arc, in the easternmost sector of the transverse Calama–Olacapato–El Toro fault zone. The magmatic rocks of the Las Burras–Almagro–El Toro complex comprise a monzogabbro to monzogranite laccolith like intrusion and basaltic andesite to dacite volcanic rocks that include seven lithostratigraphic members. New Rb-Sr dates indicate that the intrusive rocks are ca. 14 Ma, and K-Ar dates suggest emplacement ages of ca. 12.8–6.4 Ma for the volcanic rocks. The emplacement of the intrusion was controlled by N-S–striking strike-slip faults in a context of oblique convergence; the volcanism, which occurred along WNW-ESE– and N-S–striking extensional faults, relates to the Calama–Olacapato–El Toro fault zone. Two magmatic phases were recognized. Intrusive and volcanic rocks of the older magmatic phase (ca. 14–13 Ma) are characterized by Ba/Nb (7–14), La/Ta (11–18), and isotopic ratios ($^{87}Sr/^{86}Sr$: 0.704339–0.705281, $^{143}Nd/^{144}Nd$: 0.512713–0.512598), which are intraplate characteristics. The source of the older magmas was isotopically depleted lithospheric mantle rich in K, Rb, and Th. Energy constrained–assimilation and fractional crystallization (EC-AFC) modeling indicates that fractional crystallization and crustal assimilation moderately modified magma composition during its residence in the crust. The products of the younger magmatic phase (ca. 11–6 Ma) have higher Ba/Nb (24–42) and La/Ta (24–30) and $^{87}Sr/^{86}Sr$ (0.706738–0.708729) and lower $^{143}Nd/^{144}Nd$ (0.512433–0.512360). The results of EC-AFC modeling exclude a significant role for the upper crust in the generation of the most primitive magmas of this phase. Their compositions can be explained by (1) contamination of the primary magmas having originated in a depleted mantle with a mafic crust, or (2) the contribution of isotopically enriched mantle zones. Shallow differentiation and moderate contamination by continental crust can explain the composition

[†]E-mail: mazzuoli@dst.unipi.it

GSA Bulletin; November/December 2008; v. 120; no. 11/12; p. 1493–1517; doi: 10.1130/B26109.1; 16 figures; 5 tables; Data Repository item 2008123.

of the intermediate and evolved products of the younger phase. The variation of the magma source characteristics at 11 Ma is discussed in the frame of the complex geodynamical setting in this region.

Keywords: Central Andes, Eastern Cordillera, backarc magmatism, volcanic stratigraphy, geochronology, structural geology.

INTRODUCTION

An understanding of the structural context and the petrochemical features of magmas is crucial in defining the geodynamic evolution of an area. Tectono-magmatic relationships are well established in divergent oceanic and continental settings, and enable definition of consistent geodynamic scenarios (e.g., Gudmundsson, 1998; Ebinger and Casey, 2001); in contrast, knowledge of the tectonic evolution at convergent settings is more limited. It is commonly accepted that, at continental active margins, the main arc location depends on the dip of the slab and the thermal regime in the slab-wedge configuration (e.g., Stern, 2002). At shallow crustal levels, in oblique convergence settings, the volcanoes along the arc are controlled by the activity of strike-slip faults related to the partitioning of deformation (Glazner, 1991; Tikoff and Teyssier, 1992; Tobisch and Cruden, 1995; Tikoff and de Saint Blanquat, 1997; de Saint Blanquat et al., 1998). However, the shallow structural control on volcanoes behind the arc, where extensional, strike-slip, or compressional structures may form complex deformation patterns, is less well constrained. The Andean orogen is a spectacular example of convergence, mountain building, and magmatism in an active ocean-continent subduction setting, and hence represents an ideal site for investigating problems concerning the genesis and emplacement of magmas in a backarc setting.

The Central Andes have the greatest width and crustal thickness along the axis of orogen and are the result of a complex geological and magmatic evolution. The present magmatic arc, which has evolved from Miocene time onward, lies in the Western Cordillera (Fig. 1A) and forms a continuous belt of calc-alkaline stratovolcanoes and calderas. Between 21°S and 28°S, the N-S–striking Andean belt is crosscut by NW-SE strike-slip fault systems, which are associated with Miocene–Quaternary magmatism that extends far behind the main magmatic arc (Fig. 1B). The complex magmatism along these transverse structures is distinct from that of the Miocene–Quaternary volcanic arc (Coira et al., 1993; Riller et al., 2001; Matteini et al., 2002a, 2002b). The Calama–Olacapato–El Toro fault system (~24°S) is the longest of these transverse structures in the Central Andes, with inferred transtensive sinistral motion (Riller and Oncken, 2003), and is identified by the alignment of magmatic centers (e.g., Matteini et al., 2002a, 2002b; Fig. 1B). The study area is the easternmost portion of this fault, within the Eastern Cordillera, and comprises the Miocene Las Burras–Almagro–El Toro magmatic complex (Figs. 1B and 1C). The Las Burras–Almagro–El Toro magmatism is of particular interest because of (1) its position ~300 km east of the arc and ~600 km east of the trench, and (2) its occurrence within the Eastern Cordillera, which was characterized by Miocene–Quaternary compression (Marrett and Strecker, 2000; Riller and Oncken, 2003). Our reconstruction, integrating stratigraphic, structural, volcanological, petrographic, geochemical, and geochronological data sets, relates to the geology of the area and the genesis, evolution, and emplacement mechanisms of the magmas so far behind the main arc.

GEOLOGICAL SETTING

The Cenozoic Andean Cordillera and magmatic arc are the result of moderately oblique convergence between the Farallon-Nazca and South American plates (angle of ~20° between the plate motion vector and the plate boundary normal; Dewey and Lamb, 1992; Scheuber and Reutter, 1992; Fig. 1A). Complex and widespread arc magmatic activity has accompanied the evolution of the Andean margin since Mesozoic time. In the Central Andes the Jurassic–Cretaceous volcanic arc was emplaced in the present Coastal Cordillera and Chilean Precordillera. The arc migrated progressively eastward to the present Western Cordillera during the Miocene to Quaternary (Fig. 1A). East of the Miocene–Quaternary volcanic arc the Altiplano-Puna region forms a ~4000-m-high plateau (Figs. 1A and 1B) that represents the thickened axis of the orogen. East of the plateau the Eastern Cordillera consists of a W-dipping, basement-involved thrust system, which has also developed, with eastward migration, during the Miocene to Quaternary (Marrett et al., 1994; Drozdzewski and Mon, 1999; Giese et al., 1999; Scheuber and Giese, 1999; Reynolds et al., 2000; Riller et al., 2001). Farther to the east, at ~24°S, the mountain-front belt is represented by the thick-skinned Santa Barbara thrust system and the Chaco Plain foreland basin (Figs. 1A and 1C), both developed over the underthrusting Brazilian Shield (Omarini and Götze, 1991; Horton and DeCelles, 1997; Babeyko and Sobolev, 2005).

The Central Andes are crosscut by NW-SE–trending fault systems, extending from the Pacific coast as far as 400–600 km inland (Fig. 1B; Allmendinger et al., 1983; Salfity, 1985; Marrett et al., 1994). Although the database for the geometric and kinematic features of these transverse faults is limited, they have been interpreted as old, probably Paleozoic, left-lateral structures that were reactivated by the oblique convergence between the Nazca and South American plates (Riller et al., 2001; Riller and Oncken, 2003). Extensive Miocene–Quaternary magmatic activity developed along these fault systems in arc and backarc settings and formed transverse volcanic chains. Magmatism related to the NW-SE–trending Calama–Olacapato–El Toro fault system (~24°S; Fig. 1B) has occurred between 17 Ma and the Quaternary, with maximum activity between 10 and 5 Ma (Kay et al., 1999; Petrinovic et al., 1999, 2005; Matteini et al., 2002a, 2002b; Hongn et al., 2002; Haschke and Ben-Avraham, 2005). This intense magmatic activity occurred concomitantly with a strong uplift and deformation in the northern Puna and the Eastern Cordillera and coincided with an eastward shift of the compression from the plateau to the foreland (Gubbels et al., 1993). The volcanic belt along the Calama–Olacapato–El Toro structure comprises stratovolcanoes (mainly in the western Puna) and large calderas with widespread ignimbrite sheets and intrusions (mainly in the eastern Puna). The magmatic products are variable in age and in geochemical characteristics from the active volcanic arc to the Eastern Cordillera. The variations reflect different magma sources and crustal thicknesses (Matteini et al., 2002a, b). The Pliocene–Quaternary monogenetic and mainly basaltic-andesite centers emplaced in the Altiplano-Puna Plateau may relate to lithospheric delamination (e.g., Coira and Kay, 1993; Kay et al., 1994; Heit et al., 2005) in an extensional regime, active since ca. 3–4 Ma (Cabrera et al., 1987; Marrett and Emerman, 1992; Marrett et al., 1994; Kay et al., 1994).

GEOLOGY, AGE, AND STRATIGRAPHY OF THE LAS BURRAS–ALMAGRO–EL TORO MAGMATIC COMPLEX

The Las Burras–Almagro–El Toro magmatic complex encompasses an area of ~800 km^2 in the easternmost sector of the Calama–Olacapato–El Toro fault zone, ~24°35′S, 65°50′W, within the Eastern Cordillera (Figs. 1 and 2). A general petrological, geochemical, and geochronological description was previously published (Krallmann, 1994; Tubia et al., 1999; Hongn et al., 2002; Matteini et al., 2005a, 2002b). Hongn et al. (2002) reported ages of 14.4 ± 0.3 Ma (U/Pb on zircon) for the Las Burras intrusion.

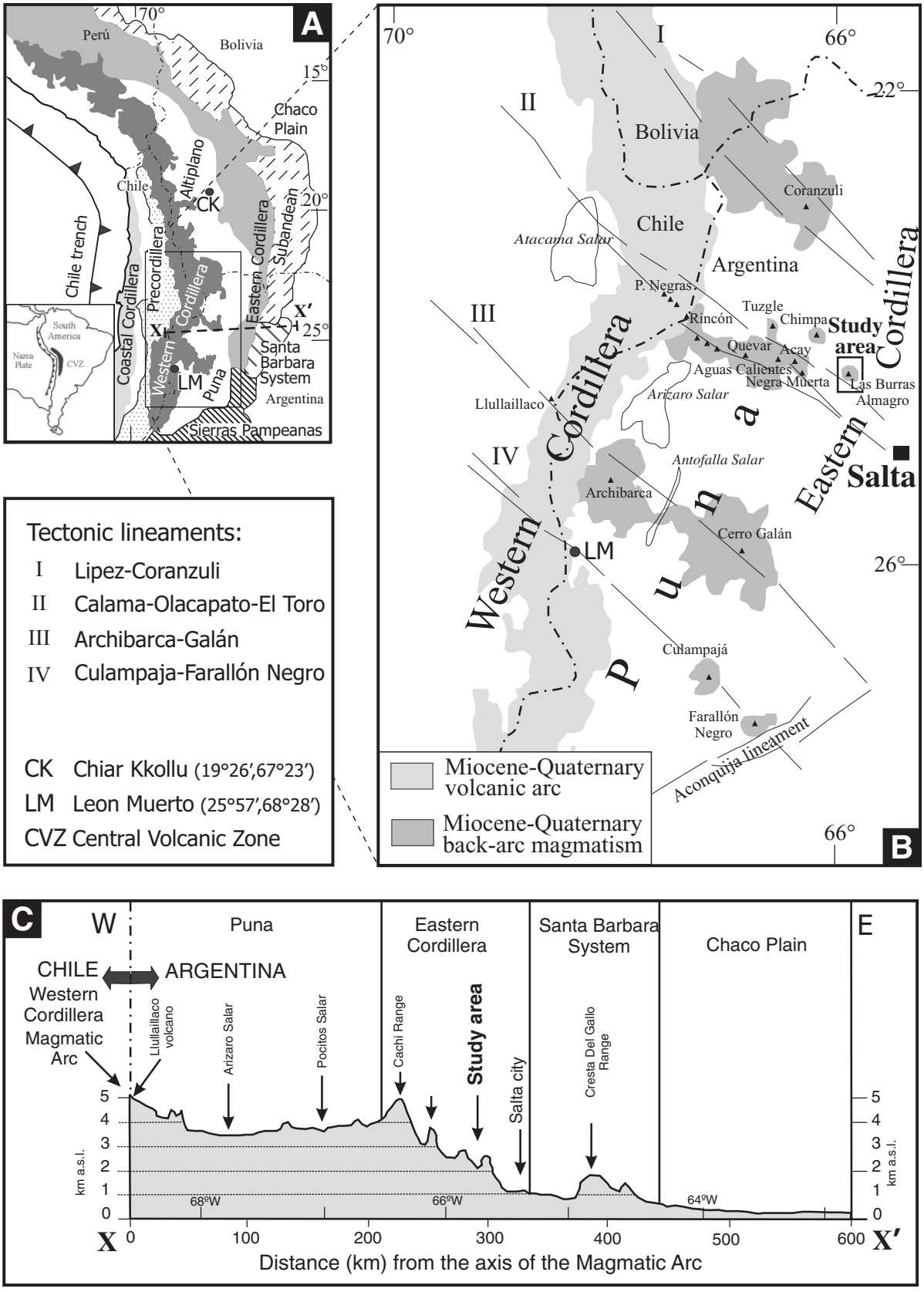

Figure 1. (A) Structural units of the Central Andes. (B) Simplified tectonic map of the southern Central Andes, showing the main structures and volcanic centers. Small rectangle indicates the study area (see Figs. 2 and 7). (C) Topographic profile at 24°47′S (dashed line X–X′ in 1A) from the magmatic arc to the foreland, modified from Malamud et al. (2002).

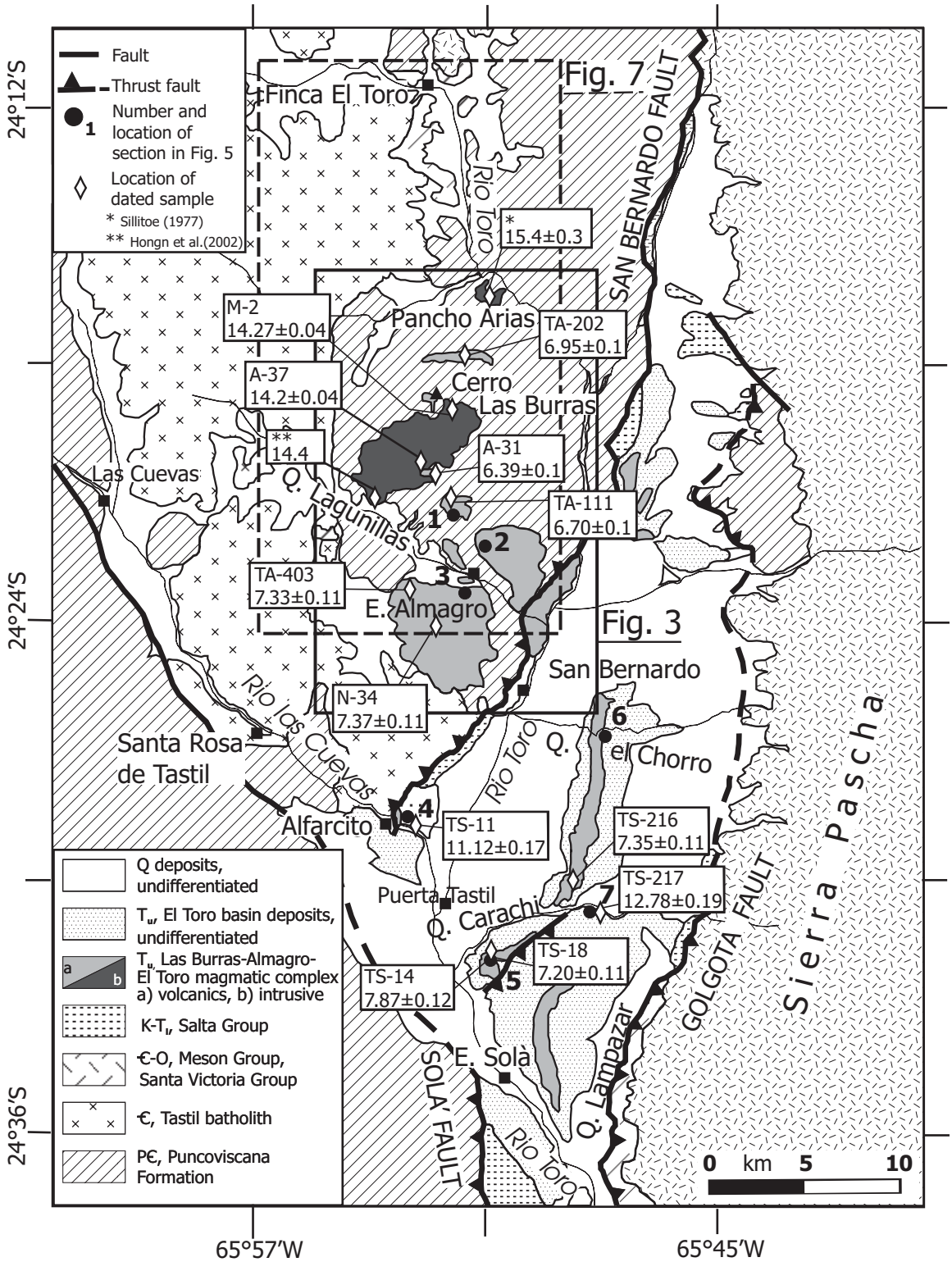

Figure 2. Geological map of the Las Burras–Almagro–El Toro magmatic complex and the El Toro basin, showing location of dated samples (ages in Ma) and stratigraphic sections. Rectangles indicate the areas in Figures 3 and 7. Numbers of samples are as in Table 2; asterisk (*) denotes age after Sillitoe (1977); double asterisk (**) denotes age after Hongn et al. (2002). Q.—quebrada (valley); E.—Estación (railway station).

In the study area (Fig. 2) the basement consists of the low-grade metasedimentary sequence of the Neoproterozoic Puncoviscana Formation (quartzite sandstones and siltstones; Mon, 1999; Omarini et al., 1999). This unit is intruded by the late Precambrian–Early Cambrian Santa Rosa de Tastil batholith (gray granodiorite and red granite; Kilmurray and Igarzabal, 1971) and by dacitic porphyry (Hongn et al., 2005). The Puncoviscana Formation is unconformably overlain by the Upper Cambrian Meson Group (whitish quartzite; Sanchez and Salfity, 1999) and the Lower Ordovician Santa Victoria Group (sandstone and green fossiliferous siltstone; Salfity et al., 1984). The Cretaceous–Paleogene Salta Group (reddish continental sandstone and shallow marine limestone and marl; Marquillas et al., 2005) unconformably overlies the Precambrian basement and Paleozoic units. In the SE sector of the study area the Las Burras–Almagro–El Toro volcanic products are intercalated with the Tertiary sediment of El Toro basin (Fig. 2; Schwab and Schafer, 1976; Marrett et al., 1994; Marrett and Strecker, 2000; Hilley and Strecker, 2005).

Structurally the area is dominated by ~N-S–trending thrusts, with slight variations in strike. Two of these opposite-verging thrust zones (San Bernardo and Golgota faults) border the El Toro basin to the west and east respectively, defining a thrust-bounded basin associated with two main directions of compression, WNW-ESE and WSW-ENE (Fig. 2; Marrett et al., 1994; Marrett and Strecker, 2000). The presence of NW-SE–trending fault systems, the possible surface expression of the Calama–Olacapato–El Toro fault zone, is suggested by the orientations of several valleys (e.g., quebrada Lagunillas; Fig. 2). These NW-SE lineaments may have been associated with the emplacement of the Las Burras pluton in a context of overall left-lateral transtension (Hongn et al., 2002).

Field mapping and stratigraphic, structural, sedimentological, and volcanological studies have been used to reconstruct the lithostratigraphic sequence and emplacement mechanisms of the Las Burras–Almagro–El Toro magmatic complex. This reconstruction includes a correlation of the magmatic and sedimentary sequences between the Las Burras–Almagro Range and the El Toro basin (Figs. 3 and 4). Rb-Sr and K/Ar age determinations were also carried out on intrusive and volcanic rocks (Tables 1 and 2). Geochronological and geochemical analytical methods are described in the Appendix.

The Las Burras–Almagro–El Toro magmatic complex consists of seven lithostratigraphic members. The oldest one is represented by the Las Burras intrusion and the others by the Almagro volcanic rocks, which are subdivided into Puerta Tastil, La Cuevas, Lampazar, and Almagro A, B, C members (Table 3). In the Las Burras–Almagro Range the Almagro volcanic products unconformably overlie the Puncoviscana Formation and Las Burras intrusion (Figs. 4 and 5). Farther east the Almagro members include both primary volcanic units and resedimented volcaniclastic deposits interbedded in the Tertiary continental clastic sequence of the El Toro basin (Figs. 3–5). For the sedimentary sequence of the El Toro basin, we adopt the stratigraphic nomenclature proposed by Marrett et al. (1994), Marrett and Strecker (2000), and Hilley and

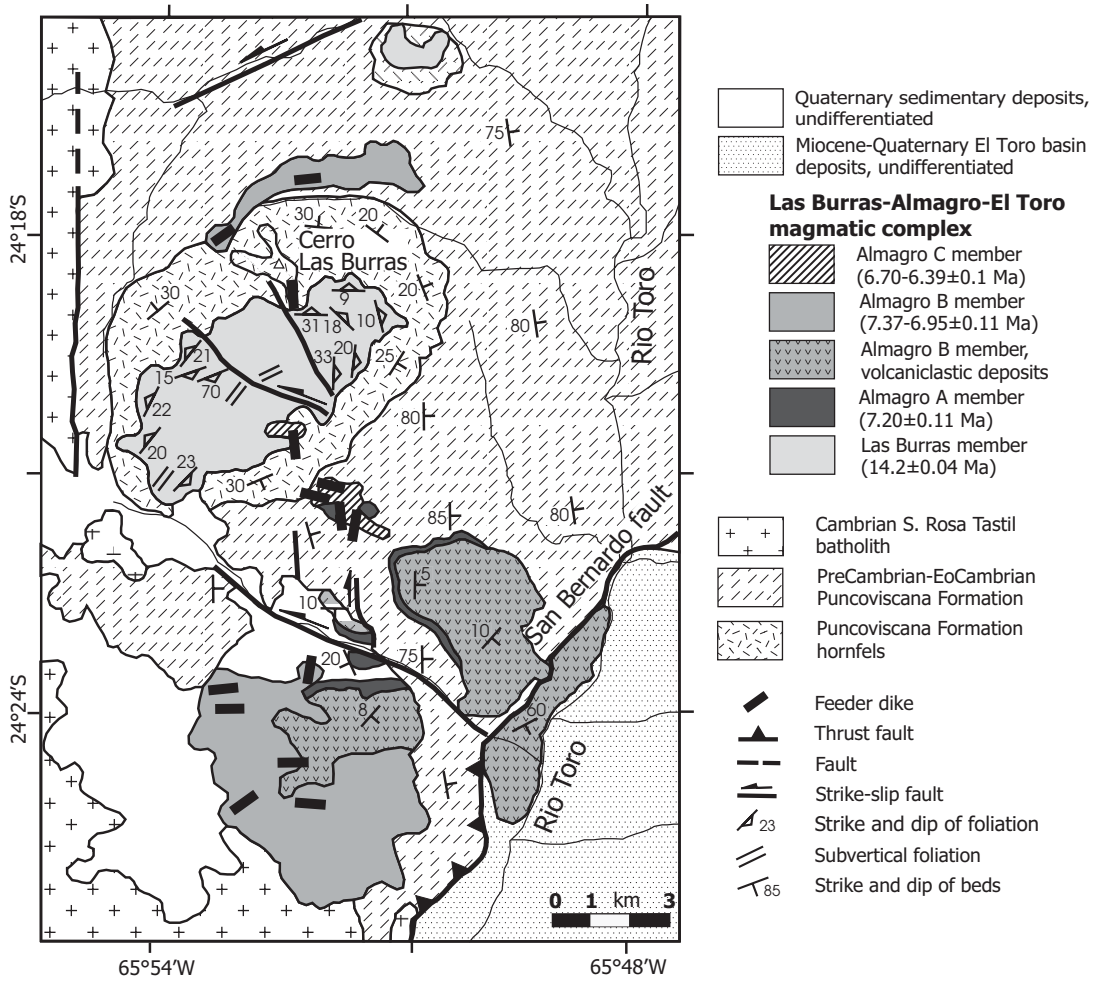

Figure 3. Geologic map of the Las Burras–Almagro Range, showing the relations between the basement rocks and the Las Burras–Almagro–El Toro magmatic complex. In the Las Burras intrusive body the strike and dip of the foliation reveal the laccolith structure.

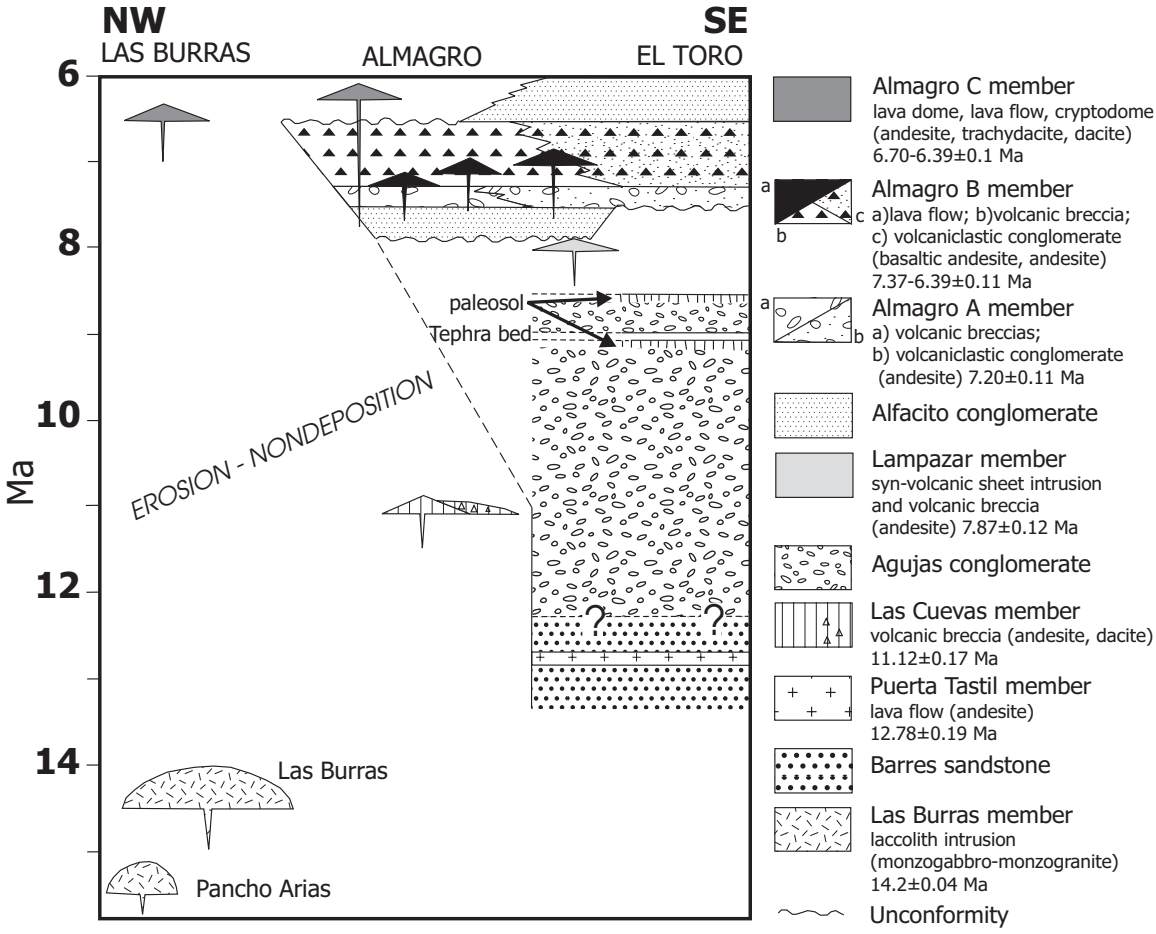

Figure 4. Chronostratigraphic framework showing the relations between the lithostratigraphic members of the Las Burras–Almagro–El Toro magmatic complex, described in the text, with the clastic sediments of the El Toro basin. Sedimentary units are from Marrett and Strecker (2000) and Hilley and Strecker (2005). In the NW sector the Almagro C member lavas directly overlie the Las Burras intrusion. In the SE sector the Las Burras–Almagro–El Toro volcanic members are interlayered in the sedimentary sequence of the El Toro basin.

TABLE 1. RB-SR GEOCHRONOLOGICAL DATA FOR LAS BURRAS ROCKS

Sample	Rb (ppm)	Sr (ppm)	$^{87}Rb/^{86}Sr$	$^{87}Sr/^{86}Sr$	$2s_m$
Monzodiorite A37 (below the erosional contact with volcanics; southern zone)					
Whole rock	158.9	666.6	0.689	0.704681	0.000012
Plagioclase	11.4	995.7	0.0331	0.704558	0.000013
Biotite	685.7	9.89	201.1	0.745101	0.000042
Age = 14.20 Ma ± 0.04; model 1 solution (±95% conf.) on 3 points					
Initial $^{87}Sr/^{86}Sr$ = 0.70455 ± 0.000069; MSWD = 0.03; probability = 0.86					
Monzodiorite M2 (top of intrusion; near northern contact)					
Whole rock	164.7	553.1	0.861	0.704862	0.000010
Plagioclase	10.7	907.8	0.0341	0.704713	0.000012
Biotite	691.2	8.71	230.9	0.751469	0.000035
Age = 14.27 Ma ± 0.04; model 1 solution (±95% conf.) on 3 points					
Initial $^{87}Sr/^{86}Sr$ = 0.70469 ± 0.000069; MSWD = 0.06; probability = 0.80					

Note: Isochrons calculated by the Isoplot/Ex program, v. 3.00; Ludwig (2003). Analytical methods in Appendix. MSWD—mean square of weighted deviates.

TABLE 2. K/Ar GEOCHRONOLOGICAL DATA FOR ROCKS OF ALMAGRO VOLCANIC UNITS

Sample	Member	K* (wt%)	Weight molten (g)	^{40}Ar* (%)	^{40}Ar* (10–11 moles/g)	Weighted mean (10–11 moles/g) ± 1σ	Age (Ma) mean value ± 2σ
A-31	Almagro C	3.105 ± 0.031	1.16356	64.208	3.477	3.449 ± 0.012	6.39 ± 0.10
	" "		0.95793	60.492	3.422		
TA-111	Almagro C	3.072 ± 0.003	1.10540	64.340	3.644	3.576 ± 0.013	6.70 ± 0.10
	" "		1.07352	60.442	3.514		
TA-202	Almagro B	2.930 ± 0.029	1.03705	63.658	3.564	3.539 ± 0.013	6.95 ± 0.10
	" "		1.03995	66.809	3.516		
TA-403	Almagro B	3.702 ± 0.037	0.97787	66.089	4.708	4.718 ± 0.017	7.33 ± 0.11
	" "		1.01487	62.618	4.728		
TS-216	Almagro B	3.545 ± 0.035	0.94488	54.702	4.496	4.526 ± 0.017	7.35 ± 0.11
			0.84713	43.555	4.557		
N-34	Almagro B	2.175 ± 0.022	1.10587	54.400	2.762	2.784 ± 0.010	7.37 ± 0.11
	" "		1.17846	53.332	2.807		
TS-18	Almagro A	2.175 ± 0.022	0.98980	40.666	2.720	2.720 ± 0.009	7.20 ± 0.11
	" "		0.98107	46.807	2.721		
TS-14	Lampazar	2.831 ± 0.028	0.94329	53.253	3.880	3.875 ± 0.014	7.87 ± 0.12
	" "		1.01518	44.793	3.869		
TS-11	Las Cuevas	2.499 ± 0.025	0.91097	20.293	4.793	4.836 ± 0.018	11.12 ± 0.17
	" "		0.26161	19.495	4.879		
TS-217	Puerta Tastil	3.512 ± 0.035	0.85457	53.190	7.847	7.808 ± 0.028	12.78 ± 0.19
	" "		0.60485	49.836	7.770		

Note: Analytical methods in Appendix.

TABLE 3. SUMMARY OF LITHOFACIES CHARACTERISTICS AND INTERPRETATION OF THE LAS BURRAS–ALMAGRO–EL TORO VOLCANIC MEMBERS

Age (Ma)	Thickness	Lithofacies	Textures and structures	Interpretation
Almagro C member				
6.39 ± 0.10 6.70 ± 0.10	30–100 m	Coherent andesite, trachydacite, and dacite	Sparsely porphyritic; vitrophyric groundmass; columnar jointed; steep-sided dome-shaped mounds or thick sheet flow; up-doming of overlying rock	Lava domes, lava flows, and cryptodomes
Almagro B member				
6.95 ± 0.10 7.33 ± 0.11 7.35 ± 0.11 7.37 ± 0.11	40–160 m	Coherent andesite	Microcrystalline or aphyric, some scoriaceous; columnar jointed, massive or flow-banded; subvertical foliation and joints in feeder zone	Lava flows and lava domes
		Monomictic andesite breccia	Nonstratified; clast-supported; poorly sorted; blocky clasts (2–60 cm); scoriaceous and flow-banded clasts common; gradational into coherent facies	Autobrecciated lava flows and lava domes
		Polymictic volcaniclastic coarse breccia and conglomerate	Roughly stratified; matrix- to clast-supported; poorly sorted; massive, normal, or inverse graded; angular to subangular clasts of microphyric to vitrophyric lavas; lithic and crystal rich, sandy or granular matrix	Volcanic debris-avalanche, debris flow, and lahar
Almagro A member				
7.20 ± 0.11	15–100 m	Monomictic andesite breccia	Matrix supported, poorly sorted, inverse-normal graded; subangular to subrounded clasts (5–10 cm , max. 200 cm) of juvenile andesite; flow banded, vitrophyric and pumiceous clasts common; vitric and crystal rich, coarse ashy and granular matrix	Block-and-ash flow, from gravitational collapse of subaerial lava dome
		Polymictic volcaniclastic conglomerates and sandstones	Globular or tubular pillowlike fluidal juvenile andesite clasts, with radial and concentric joints, glassy quenched rims; dispersed in roughly stratified, ungraded, massive conglomerate beds, 2–10 m thick; clasts of basement-derived rocks and lavas; interlayered with fine to coarse sandstone with pumiceous matrix	Dispersed peperite in coarse volcaniclastic deposits
Lampazar member				
7.87 ± 0.17	30 m	Coherent andesite	Massive, evenly porphyritic; fingerlike protusions; gradational into pillow lobes and tightly packed jigsaw-fit fragments	Coherent facies of synvolcanic sheet intrusion
		Sediment-matrix volcaniclastic breccia	Massive; poorly sorted; blocky and globular juvenile andesite clasts; well-rounded pebbles of basement rocks and nonjuvenile lavas; coarse sandstone and fine conglomerate matrix; jigsaw-fit texture; gradational into coherent facies	Peperite from sheet intrusion in coarse volcaniclastic deposits
		Polymictic pumice-matrix breccia and sandstone	Stratified, massive to diffusely planar; rounded to subangular clasts of basement rocks and lavas, in a granular pumiceous matrix	Resedimented syneruptive pyroclastic deposits in alluvial setting
Las Cuevas member				
11.12 ± 0.17	~70 m	Monomictic andesite breccia	Clast to matrix supported; massive or normal graded beds; subrounded, vesicular to pumiceous, porphyritic juvenile clasts; blocky, angular, flow-banded, vitrophyric and aphanitic juvenile clasts; coarse ashy and granular lithic matrix	Block-and-ash flow, from gravitational collapse of subaerial lava dome
		Monomictic pillow breccia	Nonstratified; poorly sorted; jagged pillow lobes (0.5–3 m) of vitrophyric juvenile andesite with radial columnar joints; granular hyaloclastic matrix; jigsaw-fit texture	Pillowed lava flow flowing into water
		Polymictic volcanic breccia	Very thick (2–4 m), internally massive beds; poorly sorted; clast to matrix supported; subrounded pillow lobes with radial joints, perlitic textures, and glassy margins; angular polyhedral glassy juvenile clasts; foliated obsidian; granular-sandy hyaloclastic matrix; jigsaw-fit texture	Syneruptive resedimented from gravity-driven failure of unstable hyaloclastic and autoclastic breccia from probably subaqueous margin of lava dome
		Stratified tuff and pumice tuff-breccia	Whitish fine and coarse ash, crystal- and glass-rich, massive or planar laminated; monomictic white pumice breccia, massive, matrix supported	Pyroclastic surge and pyroclastic flow
Puerta Tastil member				
12.78 ± 0.19	~30 m	Coherent andesite	Porphyritic; poorly vesiculated; in tabular sheets	Lava flows, vents not preserved

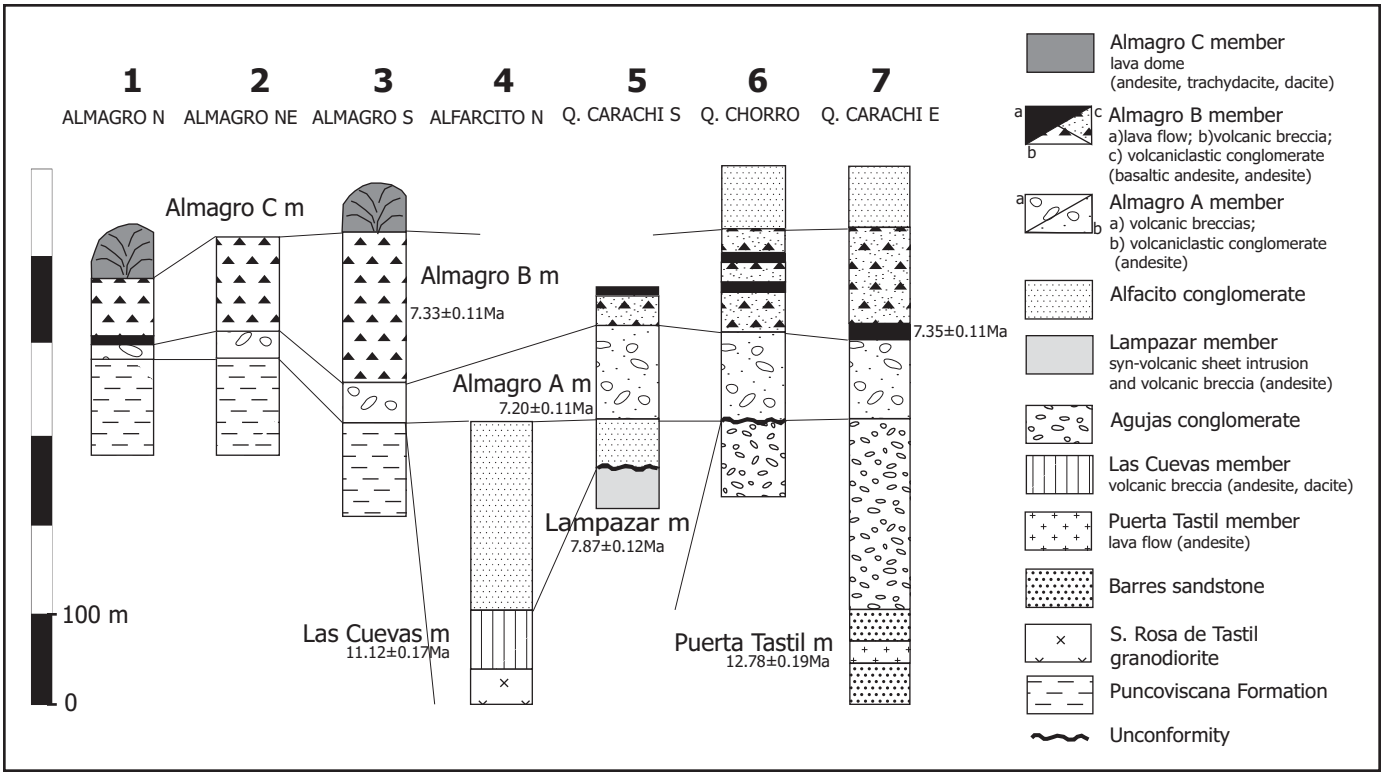

Figure 5. Selected stratigraphic sections in the Las Burras–Almagro–El Toro region (location in Fig. 2), showing correlation of the Almagro volcanic members and the El Toro basin succession in a NW-SE transect. Symbols of stratigraphic units are as in Figure 4. Sedimentary units are from Marrett and Strecker (2000) and Hilley and Strecker (2005).

Strecker (2005) (Fig. 4). These authors proposed age constraints for the Barres sandstone and the Agujas conglomerate (>8 Ma) and for the lower Alfarcito conglomerate (8–4.17 Ma), based on radiometric dating from intercalated tuffs within the sedimentary sequence.

Las Burras Member

The intrusive rocks are represented by the Las Burras member, first recognized by Hongn et al. (2002), who identified three separate bodies: Las Burras, Pancho Arias, and La Lagunilla plutons. The La Lagunilla pluton is not included in this study because our field evidence indicates that it is part of the late Precambrian–Early Cambrian Santa Rosa de Tastil batholith. The Pancho Arias stock (Figs. 2 and 3) has yielded a K/Ar age of 15.4 ± 0.3 Ma (Sillitoe, 1977). Its pervasive hydrothermal alteration precludes any further interpretation. Las Burras is an elliptical intrusion, elongated NE-SW, ~3.5 × 7 km wide (Figs. 2 and 3). Previous U-Pb dating (14.4 Ma; Hongn et al., 2002) has been confirmed by the new Rb-Sr three-point isochron ages of 14.20 ± 0.04 Ma (top of intrusion) and 14.27 ± 0.04 Ma (intermediate part of intrusion; Fig. 2 and Table 1). This pluton intruded the Puncoviscana Formation and formed a thermometamorphic aureole of pelitic hornfels (Figs. 6A and 6B). The intrusion has a magmatic foliation, given by mechanical anisotropies (i.e., fractures, Figs. 3 and 6A), with small-scale magmatic layering 0.2–1.5 m wide, highlighted by variations in the content of feldspar crystals. The foliation, spaced every few tens of centimeters to a few meters, represents a first order anisotropy within the pluton (Fig. 3). The foliation highlights the domed shape of the pluton, with a preferred NE elongation. In the southern sector the foliation is subvertical in the central part and then symmetrically diverges toward the NW and SE (Fig. 3). In the same area the pluton intrudes the Puncoviscana Formation along a planar, formerly subhorizontal contact at the base (Fig. 6A). In the northern sector the foliation defines three NE-SW–elongated, concentric shells (Figs. 3 and 6B). The Puncoviscana Formation at the contact with the intrusion has a radial attitude, with a gentle outward dip, that is concordant with the pluton foliation (Figs. 3 and 6A).

Volcanic Members

The oldest volcanic unit, the Puerta Tastil member (12.78 ± 0.19 Ma; Table 3), consists of lava flows interlayered with reddish sandstone and siltstone of the Barres sandstones (section 7 in Figs. 2 and 5; Marrett and Strecker, 2000; Hilley and Strecker, 2005).

The Las Cuevas member (11.12 ± 0.17 Ma; Table 3) is represented by lithic-rich volcanic breccia interlayered with stratified fine and coarse ash and pumice breccia. It nonconformably overlies the late Precambrian–Early Cambrian Santa Rosa de Tastil gray granodiorite and is unconformably covered by nonvolcanic conglomerate and sandstone (section 4 in Figs. 2 and 5) referred to as the Alfarcito conglomerate (Marrett and Strecker, 2000; Hilley and Strecker, 2005). Clasts of the Alfarcito conglomerate are mainly black siltstone (Puncoviscana Formation) and, subordinately, red granite (Santa Rosa de Tastil batholith). The Las Cuevas member is tilted and folded along the San Bernardo fault (Fig. 2; Marrett et al., 1994; Marrett and Strecker, 2000), which has thrust the Santa Rosa de Tastil gray granodiorite (late Precambrian–Early Cambrian) over the Miocene volcanic and sedimentary deposits of the El Toro basin (Fig. 2). Minor normal faults deformed the contacts among the Las Cuevas member, Alfarcito conglomerate, and Precambrian gray granodiorite.

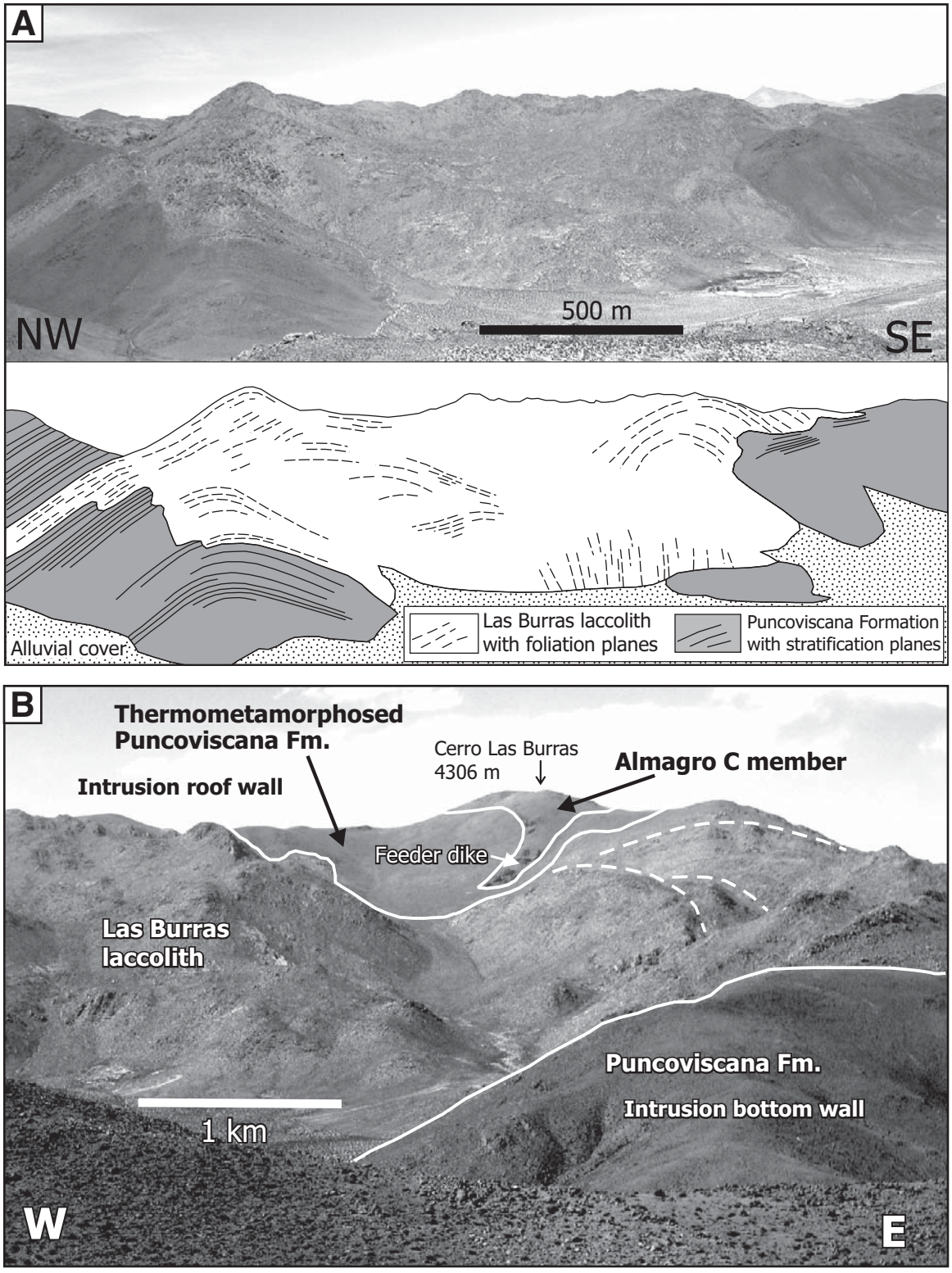

Figure 6. Views of significant outcrops of Las Burras–Almagro–El Toro members. (A) Southern side of the Las Burras laccolith, showing the main magmatic foliation planes within the intrusion (see Fig. 3 for their strike and dip). Subvertical fractures denote the flow direction of magma in the central feeding area. The foliation symmetrically diverges toward the NW and SE and highlights the domed shape of the pluton. At the base of the intrusion the foliation is subparallel to the contact with the host rock. (B) Las Burras intrusion, from SE, showing the rims of the concentric shells (dashed lines) at the NE side (Fig. 3). Country rock is the metasedimentary Puncoviscana Formation, with a thermometamorphic aureole. To the right of the intrusion, lava domes and flows of the Almagro C member crop out. The feeder dike visible in the upper part of the picture contains xenoliths of the Las Burras granodiorite.

The Lampazar member (7.87 ± 0.17 Ma; Table 3) consists of a synvolcanic andesite sheet that intruded somewhat stratified lithic-rich volcaniclastic breccia, conglomerate, and sandstone (section 5 in Figs. 2 and 5). Volcaniclastic deposits are composed of juvenile andesite fragments, old lava clasts, pumice, and basement-derived clasts (siltstone of the Puncoviscana Formation, quartzite of the Cambrian Meson Group, red granite and gray granodiorite of the Santa Rosa de Tastil batholith) in a white, granular, vitreous matrix. The juvenile andesite fragments show (1) pillowlike fluidal shapes, (2) gradational contacts with the coherent andesite of the synvolcanic intrusion, (3) jigsaw-fit textures, (4) complete glassy quenched rims, and (5) fractures filled with host sediments. Moreover, around these juvenile fragments the bedding of the host sediments has been disturbed and destroyed. On the basis of these textures, the Lampazar member is interpreted as peperite (White et al., 2000; Skilling et al., 2002), resulting from interfingering and mingling between the molten andesite sheet intrusion and unconsolidated, wet, coeval volcaniclastic deposits. This member is covered by a sequence of nonvolcanic reddish conglomerates and sandstones (section 5 in Fig. 5), with an erosional contact and angular unconformity. Clasts in these sedimentary strata consist mainly of siltstone (Puncoviscana Formation) and subordinately of red granite (Santa Rosa de Tastil batholith); thus they correlate with the Alfarcito conglomerate (Marrett and Strecker, 2000; Hilley and Strecker, 2005).

The Almagro A member (7.20 ± 0.11 Ma; Table 3) consists of monomictic volcanic breccias, interbedded with polymict volcaniclastic conglomerate and sandstone (sections 1–3 and 5–7 in Fig. 5). In a NW-SE transect, the deposits exhibit lateral changes in thickness and lithofacies. The depositional characteristics vary from proximal and prevailing primary volcanic facies represented by monomictic breccias of juvenile andesite clasts in a vitric- and crystal-rich ashy matrix, 20–30 m thick, in the NW sector, to distal and resedimented volcaniclastic facies represented by 80–100-m-thick stratified volcanic breccia, conglomerate, and sandstone in the El Toro basin (Fig. 5).

In the Las Burras–Almagro Range (Fig. 3) the Almagro A member directly overlies the Puncoviscana Formation on an angular unconformity, is paraconformably covered by the volcaniclastic deposits of the Almagro B member, and is intruded by the feeder dikes of the same member. In the El Toro basin the Almagro A member overlies different clastic sedimentary deposits (Figs. 4 and 5). In the quebrada Carachi the Almagro A member is unconformable with nonvolcanic reddish conglomerate and sandstone attributed to the Alfarcito conglomerates. In the northern El Toro basin (i.e., quebrada el Chorro) this member paraconformably overlies (the contact is marked by a paleosol) polymict nonvolcanic conglomerate, the Agujas conglomerate (Marrett and Strecker, 2000).

The Almagro B member was emplaced in a narrow time span, with K/Ar ages of 7.37 ± 0.11 Ma, 7.35 ± 0.11 Ma, 7.33 ± 0.11 Ma, and 6.95 ± 0.10 Ma (Table 2). It consists of andesite lava flows, lava domes, volcaniclastic coarse breccias, and conglomerates (Table 3). This unit crops out extensively in the Las Burras–Almagro Range and El Toro basin (Figs. 3 and 5). The lava domes have originated from several WNW-ESE–aligned, small eruptive centers (Hauser et al., 2005). Most of their feeder dikes trend ~W-E; ~N-S–trending dikes are also present (Fig. 3). In some sections (Fig. 5), lava flows are interbedded with volcaniclastic breccias, which progressively predominate in the NE (Fig. 3). In the Las Burras–Almagro Range the Almagro B member paraconformably overlies the Almagro A member, whereas in the El Toro basin this contact is unconformable.

The youngest volcanic unit, the Almagro C member (6.70 ± 0.10 to 6.39 ± 0.10 Ma; Table 3), consists of andesite, trachydacite and dacite lava domes, lava flows, and cryptodomes, with feeder dikes having N-S and WNW-ESE directions (Fig. 3). The lava flows directly overlie the Las Burras intrusion (Figs. 3–5). In the northern area the feeder dike of a lava dome contains xenoliths of Las Burras granodiorite (Fig. 6B). On the northern side of the quebrada Lagunilla, cryptodomes intruded, deformed, and uplifted the Puncoviscana Formation and the volcaniclastic strata of the Almagro A and B members.

Field and geochronological data indicate that mainly effusive monogenetic centers (lava domes, cryptodomes, scoria cones with lava flows) characterized Las Burras–Almagro–El Toro volcanism between 11.12 ± 0.17 Ma and 6.39 ± 0.10 Ma. The lava flows are commonly autobrecciated. Pyroclastic rocks are rare and related to low-energy explosive eruptions, suggesting the ascent of small volumes of degassed magma. The volumes of the Almagro volcanics are difficult to estimate, given the lack of continuous outcrops. We estimate a minimum volume of ~2 km^3 for the Almagro B member, and a maximum volume of 0.2 km^3 for the Almagro C member. The lithofacies of some of the oldest volcanic deposits (the Las Cuevas, Lampazar, and Almagro A members), as autobrecciated and pillowed lava flows, quenched margin of lava domes, and peperite (Table 3), indicate magma-water interaction and the presence of a continental shallow-water environment and water-saturated sediments in the El Toro basin at the time. The structures controlling the magma emplacement are poorly exposed, except for the feeder dikes of the Almagro B and C members, which strike ~W-E, N-S, or WNW-ESE (Fig. 3).

STRUCTURAL FEATURES

Most of the present structural analysis was carried out in the Las Burras intrusion, as detailed structural measurements on the thrust faults that bound the El Toro Basin are already available (Marrett and Strecker, 2000, and references therein). The deformation around the intrusion (Fig. 7) consists largely of faults, extensional fractures, dikes, and folds. The structural data were collected in the Puncoviscana Formation, the Las Burras pluton, and the Almagro volcanics (Fig. 7).

These data show the widespread presence of strike-slip structures with ~N-S and ~NW-SE trends. The N-S–striking faults are dextral and are found mainly along the N-S–trending Rio Toro Valley, between the Finca El Toro and the Pancho Arias stock (sites 10, 11, 45, 46–47, and 48; Fig. 7). Most of these faults are found within the Puncoviscana Formation. The deformation related to these faults is concentrated along several discrete zones, each a few tens of meters wide, with a displacement of at least several tens of meters. These dextral faults are associated with NE-SW sinistral faults and concentric folds with hinges trending NW-SE (sites 10 and 11; Fig. 7). A N-S–trending dextral structure is found in the SW sector of the Almagro–Las Burras Range, within the Puncoviscana Formation and the Santa Rosa de Tastil gray granodiorite (sites 29, 30–31, and 33; Fig. 7).

The NW-SE faults are sinistral and are found mostly in the Puncoviscana Formation, along the NW-SE–trending quebrada Lagunilla, south of the Las Burras pluton (sites 21, 36, and 37; Fig. 7). Other NW-SE sinistral faults are observed within the Las Burras intrusion (sites 14–15, 23, and 41–43; Fig. 7) and along the northern Rio Toro Valley (site 48; Fig. 7).

Both dextral N-S and sinistral NW-SE faults could be related to a similar structural setting, within a context of simple shear related to an overall ~ENE-WSW compression (Sylvester, 1988).

There is widespread evidence of reactivation of the N-S– and, especially, the NW-SE–striking strike-slip faults with extensional kinematics, forming normal or transtensional faults. The NW-SE–striking structures are usually accompanied by NW-SE–trending extension fractures, which, within the Las Burras pluton, are associated with discrete mineralization (sites 16, 17, and 23; Fig. 7).

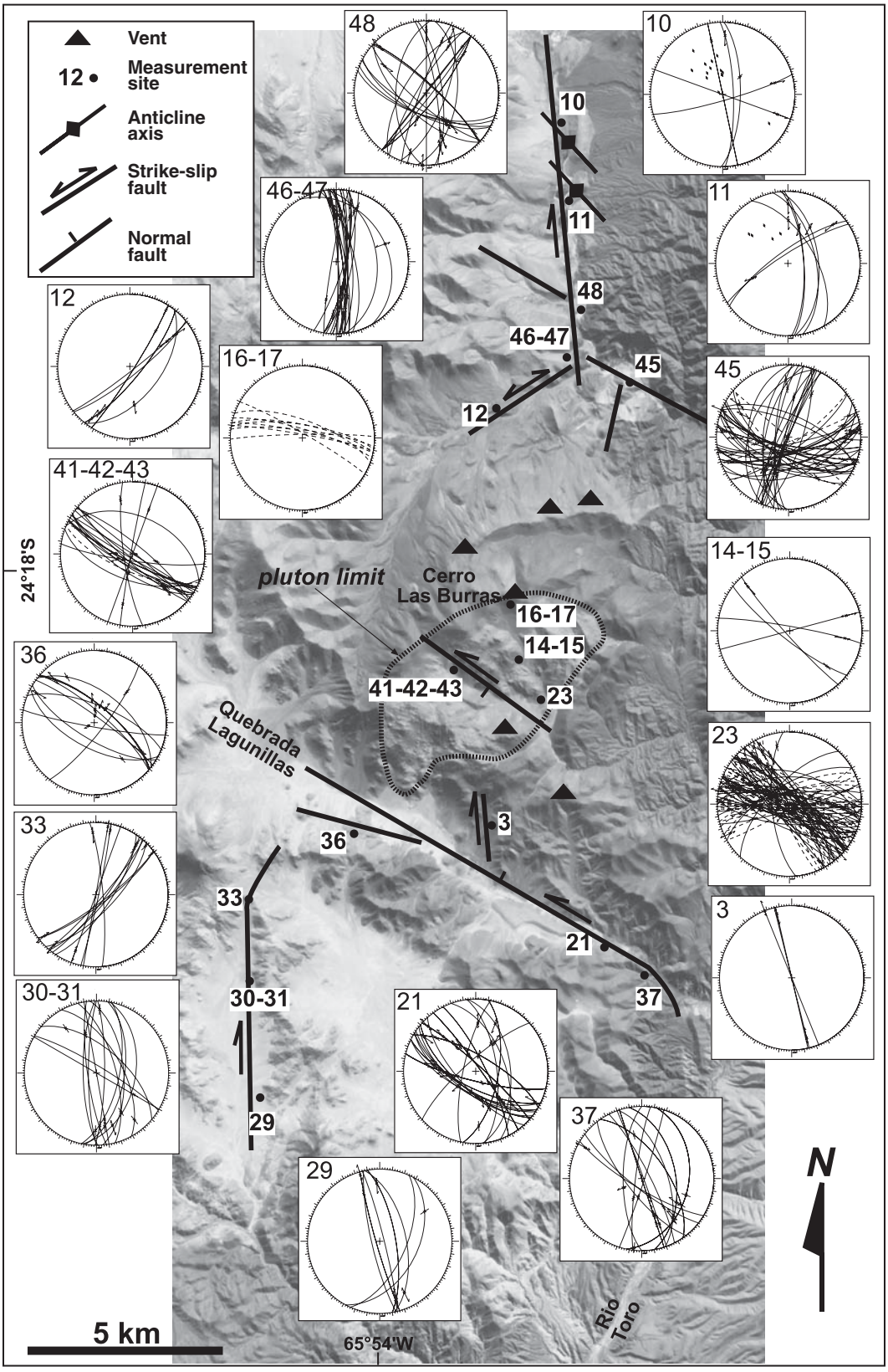

Figure 7. Structural map of the Las Burras–Almagro–El Toro magmatic complex, showing the main measurement sites. The data are plotted as a lower hemisphere Schmidt projection, subdivided by measurement sites. Solid lines—faults; dashed lines—joints; arrows within the plots—sense of movement, as inferred from striations. Numbers on stereonets are locality numbers on the map.

Marrett and Strecker (2000) suggest that these strike-slip structures relate to the Miocene–Pliocene compressive buildup of the Eastern Cordillera. This hypothesis is supported by the similar trends of the major strike-slip structures and the main morphological structures (valleys, ridges, incisions) of the area. These extensional faults postdate the ca. 14 Ma intrusion age of the Las Burras pluton, probably by a substantial interval of time, given that they represent brittle conditions; thus their age is between the middle Miocene and the Quaternary.

ROCK CLASSIFICATION, PETROGRAPHY, AND MINERAL CHEMISTRY

Las Burras Intrusion

The Las Burras rocks have an SiO_2 content in the range of 54–65 wt% (Tables 4 and DR1[1]; Fig. 8) and have compositions ranging from monzogabbro to monzogranite, according to the normative classification of Streckeisen and Le Maitre (1979). The most mafic rocks show a transitional character straddling the Irvine and Baragar (1981) curve, whereas the intermediate and silicic samples fall in the subalkaline field and classify as metaluminous calc-alkaline granitoids. The main mineral phase proportions are reported in Figure 9, with representative analyses in Table DR3 (see footnote 1). About 70% of the total outcrop area consists of monzodiorite, with plagioclase, augite pyroxene, and brown-green Mg-hornblende mainly as replacement of pyroxene. The monzogranite varieties show alkali feldspar and quartz together with plagioclase, amphibole, and biotite. Common accessory minerals are sphene, ilmenite, Ti-magnetite, zircon, and apatite.

Dispersed throughout the pluton, and particularly abundant in the SW, are enclaves, which are angular or rounded, partially remelted metasedimentary blocks of the country rock, usually found near the contact, and microgranular enclaves. The latter have a mineral assemblage of plagioclase + K-feldspar + clinopyroxene + amphibole + biotite ± quartz ± zircon ± apatite ± oxides.

Almagro Volcanic Rocks

The Almagro rocks are subalkaline (Fig. 8); their SiO_2 content ranges from 53 to 66 wt%, defining a calc-alkaline trend from basaltic andesite to dacite (Fig. 8; Tables 4 and DR2 [see footnote 1]). Rocks of the Puerta Tastil, Las Cuevas, Lampazar, and Almagro A and B members are porphyritic andesites, with plagioclase and amphibole phenocrysts, some reaching up to 1–2 cm in size. In some lavas (Lampazar, Almagro A and B), clinopyroxene is the dominant mafic phenocryst instead of amphibole. Silicic rocks occur in the Almagro C member and have a vitrophyric texture with sparse microcrystals of plagioclase, amphibole, and rare orthopyroxene. Apatite and Fe-Ti oxides are common accessories. Average phenocryst modal data are shown in Figure 9, and representative analyses are provided in Table DR3 (see footnote 1). The Almagro C member rocks commonly include xenoliths with quartz or garnet, eroded from the basement rocks during magma ascent or storage. No rocks with a mineral assemblage like that of the Las Burras intrusion were found.

Several disequilibrium features occur in the Almagro volcanic rocks. Some andesite lavas of the Puerta Tastil and Almagro B members contain magmatic enclaves of mafic magma bearing olivine and clinopyroxene phenocrysts in an isotropic groundmass. They show a quench texture of the microlites, which suggests magma mingling processes (Bacon, 1986; Snyder, 2000; Perugini and Poli, 2000). In addition, most andesites of the Almagro B member contain phenocrysts of clinopyroxene coexisting with two populations of amphibole, one showing reaction rims (indicating disequilibrium) and the other in equilibrium. This suggests the occurrence of mingling and mixing processes between magmas with anhydrous and hydrous paragenesis (Coombs et al., 2003; Coombs and Gardner, 2004, and references therein).

Basaltic andesites occur only in the Almagro B member. They are characterized by a banded texture, with dark microlite-rich bands alternating with light-colored glassy portions. In the dark bands the prevalent phenocrysts are Cr-rich clinopyroxene with high Mg# (100*MgO/[MgO + FeO_t], where FeO_t = total Fe as FeO) and sieve-textured plagioclase, whereas the light-colored bands have microcrystals of plagioclase without sieve texture, orthopyroxene, low Mg# clinopyroxene, Fe-Ti oxides, and apatite. A particularly primitive association of coarse olivine (Fo 87–83) with iddingsite rims, with small grains of Al- and Ti-rich clinopyroxene averaging $Wo_{47}Fs_{10}$ and Cr-spinel ($Cr_{\#}$ = 59–51), occurs in the dark bands (Table DR3; see footnote 1). Crystals from the dark bands occur in the clear ones and vice versa, and reverse or oscillatory zoning is common in the plagioclase, clinopyroxene, and orthopyroxene phenocrysts (e.g., up to Mg# 66 in the core to 84 at the rim in clinopyroxene; Table DR3; Fig. DR1; see footnote 1). The basaltic andesites contain clinopyroxenitic enclaves 1–3 cm in size, with clinopyroxene composition in the range $Wo_{42}Fs_{11}$-$Wo_{44}Fs_{13}$ and scarce orthopyroxene $En_{72}Fs_{25}$-$En_{74}Fs_{21}$, with, in one case, phlogopite with Mg# 74–71 and Al-Fe spinel.

GEOCHEMISTRY

Major and Trace Elements

Representative analyses of the Las Burras–Almagro–El Toro complex rocks are presented in Table 4. The complete set of analyses is provided in Table DR1 (see footnote 1), and Harker-type diagrams are shown in Figure DR2 (see footnote 1). The Las Burras and Puerta Tastil rocks show the same geochemical characteristics, whereas the Almagro volcanic rocks younger than 11 Ma (Las Cuevas, Lampazar, and Almagro A, B, and C members) define a distinct trend. The Las Burras and Puerta Tastil rocks have higher K_2O and lower MgO contents than the younger Almagro units. Al_2O_3 and Na_2O exhibit a positive correlation with SiO_2 for the Almagro rocks, whereas the Las Burras rocks show a bell-shaped pattern. CaO and TiO_2 show a compatible behavior and decrease with silica. The two groups of rocks display distinct trends, with increasing silica in many trace element diagrams (Fig. DR2; see footnote 1): the Las Burras and Puerta Tastil members have a higher Rb content, a lower and constant Ba, and a similar and scattered Sr, when compared with the Almagro younger members. Nb shows a compatible behavior in the Las Burras and Puerta Tastil rocks, and an opposite trend in younger rocks. The most silicic products are the Almagro C dacite rocks, which show remarkably high Zr and Hf contents.

The most mafic samples of the Las Burras rocks have Mg# no higher than 63 and low Ni, Co, and Cr contents. The most primitive Almagro volcanic rocks are the basaltic andesites in the Almagro B member, with Mg# = 71–75. The spider diagrams in Figure 10A illustrate the trace element composition of the most mafic samples of the complex, and are compared with other arc (Leon Muerto, Fig. 1A; Trumbull et al., 1999) and intraplate Central Andes basalts (Chiar Kkollu, Fig. 1A; Davidson and de Silva, 1995). In the spider diagrams the Las Burras and Almagro B mafic samples are approximately similar, displaying positive anomalies of Rb, Th, K, and Pb, and negative troughs of Nb, Ta, and Ti. The Las Burras intrusive rocks show higher peaks of Rb, Th, and K, and very slight Nb and Ta troughs. The rare earth element

[1]GSA Data Repository Item 2008123, major and trace element bulk rock analyses and mineral chemistry of Las Burras intrusive rocks and of Las Burras-Almagro-El Toro volcanic rocks (data and selected diagrams), is available at www.geosociety.org/pubs/ft2008.htm. Requests may also be sent to editing@geosociety.org.

TABLE 4. MAJOR AND TRACE ELEMENT ANALYSES OF REPRESENTATIVE SAMPLES OF LAS BURRAS INTRUSIVE ROCKS AND ALMAGRO VOLCANIC ROCKS

Sample	M-2	A-37	TA-104	TS302	TS 217	TS 11	TS 14	TS 18	N-32	TA-403	TA-210	TA-111
Member	Las Burras	Las Burras	Las Burras	Las Burras	Puerta Tastil	Las Cuevas	Lampazar	Almagro A	Almagro B	Almagro B	Almagro C	Almagro C
Latitude S	24°18'55"	24°20'30"	24°21'19"	24°19'56"	24°31'18"	24°29'33"	24°32'54"	24°32'50"	24°24'27"	24°22' 51"	24°18'17"	24°21'15"
Longitude W	65°52'20"	65°52'37"	65°53'52"	65°51' 36"	65°45'58"	65°53'30"	65°50'47"	65°50'31"	65°52'29"	65°51' 32"	65°53'07"	65°52'06"
SiO_2 (wt%)	61.75	55.13	64.94	61.08	60.47	59.84	56.47	61.36	53.17	61.84	55.02	61.15
TiO_2	0.69	1.01	0.41	0.66	0.76	0.78	1.04	0.67	1.14	0.76	1.28	0.60
Al_2O_3	16.69	16.83	14.06	16.46	15.30	16.85	17.11	16.05	15.02	16.62	15.80	17.72
Fe_2O_3 tot.	6.18	8.11	3.91	5.63	6.79	6.17	7.47	5.35	9.24	5.83	9.60	4.68
MnO	0.16	0.17	0.07	0.15	0.12	0.12	0.15	0.12	0.14	0.11	0.15	0.09
MgO	2.07	3.07	1.07	1.69	1.93	2.77	3.66	2.62	5.99	2.67	4.71	1.15
CaO	5.57	7.18	3.24	5.35	7.03	5.32	6.81	5.87	8.01	5.02	6.57	4.38
Na_2O	3.19	3.24	2.69	3.56	3.12	3.31	3.00	3.70	2.57	2.93	2.66	3.29
K_2O	3.70	3.49	5.08	3.53	3.45	2.65	2.82	2.43	2.55	3.69	2.70	3.64
P_2O_5	0.32	0.45	0.17	0.31	0.34	0.29	0.36	0.23	0.37	0.31	0.36	0.33
L.O.I.	0.35	0.37	0.46	0.44	1.41	1.92	1.23	1.09	1.39	1.61	0.28	0.94
Be (ppm)	2.29	2.72	3.50	2.47	2.17	2.40	2.23	1.85	1.74	2.85	1.67	2.95
Sc	10	13	6	8	12	14	22	15	23	12	24	7
V	104	168	70	90	95	120	198	123	222	108	225	42
Cr	12	26	10	9	85	34	27	114	309	50	52	5
Co	13	19	5	11	15	15	20	17	60	13	29	6
Ni	8	14	4	7	25	15	13	24	58	15	32	3
Cu	22	26	35	17	27	18	30	14	37	21	50	8
Rb	162	151	192	167	142	134	102	88	88	138	91	145
Sr	550	650	378	639	524	469	575	547	530	543	429	550
Y	25.0	26.2	16.1	23.6	22.9	24.7	29.4	17.9	25.8	22.9	30.4	24.6
Zr	162	179	114	-	77	187	182	102	147	193	169	371
Nb	31.6	32.9	23.7	36.9	29.9	19.6	22.6	13.2	20.5	24.0	19.4	23.9
Cs	7.78	5.00	3.50	4.25	4.57	6.27	4.28	2.15	4.18	8.10	3.24	7.00
Ba	418	415	341	471	380	507	573	454	565	624	425	999
La	34.5	34.0	27.2	38.7	32.4	36.8	35.7	24.9	33.1	42.0	29.3	42.0
Ce	63.5	64.0	47.0	69.8	61.3	70.9	69.2	49.2	64.5	78.0	61.0	79.0
Pr	7.3	7.7	5.2	7.9	7.1	8.3	8.1	5.9	7.9	9.1	7.5	9.2
Nd	27.7	30.1	18.5	29.0	26.6	30.4	30.9	22.2	30.9	34.0	30.0	34.0
Sm	5.3	5.9	3.5	5.4	5.1	5.9	6.0	4.4	6.2	6.2	6.5	6.0
Eu	1.45	1.75	0.84	1.43	1.31	1.28	1.39	1.05	1.57	1.47	1.59	1.37
Gd	4.6	5.1	2.9	4.7	4.5	5.0	5.7	3.8	5.4	5.0	6.1	4.8
Tb	0.72	0.80	0.44	0.69	0.70	0.77	0.85	0.57	0.83	0.76	0.95	0.72
Dy	4.1	4.6	2.5	4.0	3.8	4.3	5.0	3.1	4.5	4.1	5.5	4.1
Ho	0.83	0.90	0.52	0.81	0.78	0.83	0.99	0.62	0.89	0.80	1.09	0.82
Er	2.27	2.44	1.47	2.23	2.18	2.29	2.76	1.69	2.39	2.12	2.89	2.25
Tm	0.35	0.37	0.23	0.35	0.31	0.35	0.42	0.25	0.34	0.30	0.43	0.37
Yb	2.22	2.22	1.52	2.10	2.10	2.20	2.60	1.55	2.14	1.93	2.65	2.27
Lu	0.32	0.33	0.23	0.31	0.30	0.31	0.37	0.21	0.29	0.28	0.38	0.36
Hf	n.d.	n.d.	n.d.	n.d.	2.32	4.86	4.59	2.99	3.99	5.20	4.49	8.40
Ta	2.50	2.33	1.95	2.76	2.26	1.46	1.44	0.92	1.30	1.67	1.21	1.58
Tl	0.95	0.88	0.92	0.99	0.11	0.70	0.61	0.25	0.33	0.96	0.56	0.88
Pb	n.d.		9.1	N.D.	9.9	14.1	11.2	7.7	12.7	16.2	n.d.	14.3
Th	12.79	9.10	19.40	13.03	11.22	12.05	9.21	6.40	8.41	12.80	7.39	11.60
U	3.29	2.51	3.31	2.69	2.36	2.69	2.34	1.76	1.88	3.06	1.71	2.83
$^{87}Sr/^{86}Sr_{meas}$	0.70486	0.704688	0.70559	0.704936	0.705233	0.708509	n.d	n.d.	0.706788	0.707683	0.707965	0.708419
(±2s)	(10)	(10)	(11)	(11)	(12)	(11)			(11)	(12)	(10)	(12)
$^{87}Rb/^{86}Sr$	0.861	0.692	1.513	0.755	0.715	0.826	n.d.	n.d.	0.479	0.758	0.614	0.775
$^{87}Sr/^{86}Sr_i$	0.704685	0.704547	0.705281	0.704782	0.705103	0.708380	n.d.	n.d.	0.706738	0.707604	0.707904	0.708345
$^{143}Nd/^{144}Nd_{meas}$	0.51271	0.512696	0.512609	0.512693	0.512646	0.512374	n.d.	n.d.	0.512439	0.51242	0.512425	0.512389
(±2s)	(9)	(5)	(6)	(9)	(10)	(11)			(11)	(11)	(12)	(7)
$^{147}Sm/^{144}Nd$	0.116	0.119	0.113	0.112	0.117	0.118	n.d.	n.d.	0.121	0.119	0.131	0.109
$^{143}Nd/^{144}Nd_t$	0.512699	0.512685	0.512598	0.512682	0.512636	0.512366	n.d.	n.d.	0.512433	0.512292	0.512419	0.512384

Note: Analytical methods in Appendix. Trace elements analyzed by ICP-MS except Zr for Las Burras intrusive rocks. The complete set o f analyses is available as supplementary material in Tables DR1 and DR2. L.O.I.—loss on ignition. ICP-MS—inductively-coupled-plasma mass spectroscopy. N.D.—not determined.

(REE) patterns of the mafic samples of the Las Burras and Almagro B members are strikingly similar, except for a minor negative Eu anomaly in the latter (Fig. 10B). The Las Burras rocks show a wider range of REE abundances than the Almagro rocks younger than 11 Ma (Figs. 10C and 10D, and inset in C) and an increase of REE fractionation with silica (La/Yb from 12 to 18 for SiO_2 from 52 to 65 wt%; Table DR1; see footnote 1). A negative Eu anomaly characterizes all the Almagro rocks, and only the most evolved Las Burras sample (Figs. 10C and 10D).

Sr and Nd Isotopic Ratios

In the $^{87}Sr/^{86}Sr$ versus $^{143}Nd/^{144}Nd$ diagram (Fig. 11A) the Las Burras and Puerta Tastil rocks show the lowest Sr and the highest Nd isotopic ratios and define a negative trend. In detail, the three samples from the southern outcrops of Las Burras (feeder zone) define a cluster with relatively low Nd and high Sr isotopic ratios ($^{87}Sr/^{86}Sr$ ~0.7053; $^{143}Nd/^{144}Nd$ ~0.51259). They are distinct from the samples from the central-northern outcrops, which have $^{87}Sr/^{86}Sr$ ~0.7045 and $^{143}Nd/^{144}Nd$ ~0.51271 (see inset in Fig. 11A). The Almagro volcanic rocks younger than 11 Ma are separated from the Las Burras and Puerta Tastil rocks by a large gap in isotopic ratios, and their $^{87}Sr/^{86}Sr$ ratios range from

0.706738 to 0.708729 and $^{143}Nd/^{144}Nd$ ratios from 0.512433 to 0.512360; the basaltic andesites of the Almagro B member show the lowest Sr and highest Nd ratios. In Figure 11B the isotopic ratios are plotted against SiO_2 contents. The Las Burras samples show a very weak positive correlation between silica and Sr isotopic ratios and a negative correlation between silica and Nd. Overall, the Almagro volcanic rocks do not indicate any correlation of isotopic ratios with SiO_2 content, although patterns can be observed within the samples from individual volcanic members.

DISCUSSION

Geological Evolution

Las Burras Intrusion

The Las Burras intrusion is the oldest Cenozoic magmatic unit in the study area. Its foliation, subparallel to the magma flow, is interpreted as the mechanical expression of a discontinuity in the flow (Marre, 1986; Paterson and Vermon, 1995; Hrouda et al., 1999; Dietl and Koyi, 2002). Therefore, the strike and dip of the foliation indicate the flow directions of magma within the pluton (Ferré et al., 2002). The foliation, subparallel to the contact with the overlying host rock, suggests lateral flow of magma at the top of the intrusion. The subvertical and NE-SW–trending foliation in the center of the southernmost part suggests vertical flow (Figs. 3 and 6A). These flow directions, together with the tabular intrusion shape, thicker in the center, suggest that the Las Burras intrusion is a laccolith, elongated NE-SW, with a NE-SW–trending feeder dike in its southern part. The differences in Sr and Nd isotopic composition between the feeder zone (southern outcrop) and the main intrusive body (central-northern outcrop; see inset in Fig. 11A) could relate to distinct batches of magma feeding the laccolith. The voluminous first batches had higher Nd and lower Sr isotopic ratios than the later ones, representing a new, slightly more evolved and contaminated pulse of magma that formed the feeder zone.

The emplacement of the NE-SW–trending feeder dike at the base of the laccolith could be kinematically related to the N-S–striking dextral faults. These faults were likely active in the Miocene (see the Structural Features section) during pluton emplacement. The N-S–striking dextral faults at the NE and SW sides of the intrusion could have created a releasing bend, or a localized extensional zone, which favored the rise of magma through one or more NE-SW–trending feeder dikes (cf. Busby-Spera and Saleeby, 1990; Glazner, 1991; Tikoff and Teyssier, 1992; Tobisch and Cruden, 1995; Tikoff and de Saint

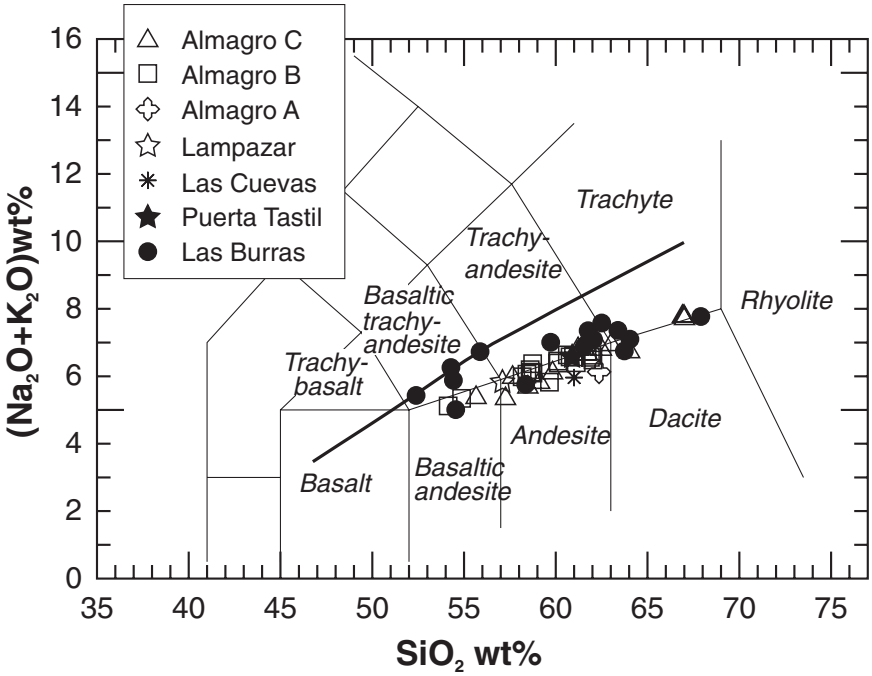

Figure 8. TAS (total alkali versus SiO_2 wt%) diagram (Le Bas et al., 1986) of Las Burras–Almagro–El Toro rocks. Heavy line (Irvine and Baragar, 1981) divides alkaline and subalkaline fields.

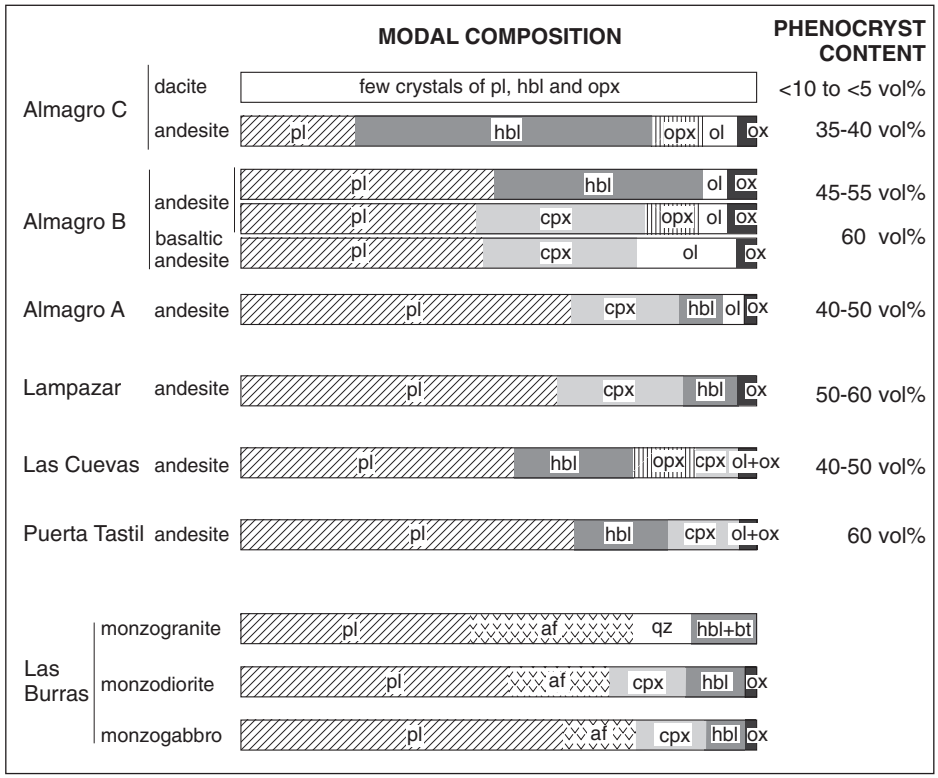

Figure 9. Mineral phase content (volume percentages) of representative samples of the Las Burras intrusion and the Almagro volcanic rocks: pl—plagioclase; af—alkali feldspar; qz—quartz; hbl—hornblende; cpx—clinopyroxene; opx—orthopyroxene; ol—olivine; bt—biotite; ox—Fe-Ti oxides.

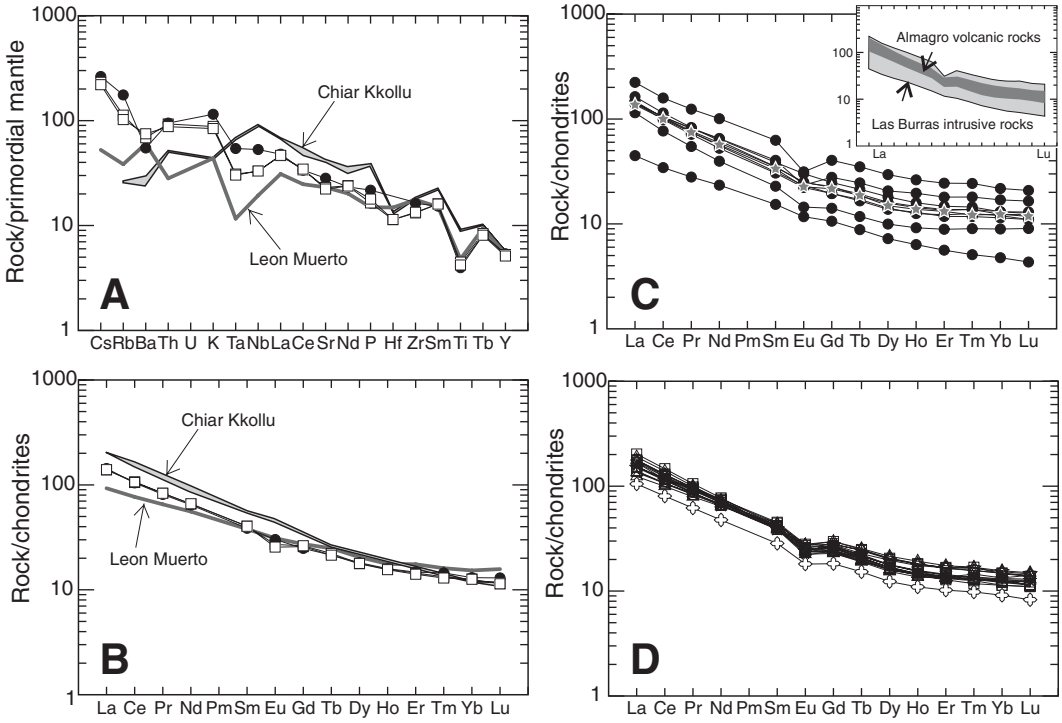

Figure 10. (A) Spider diagrams (normalized relative to primordial mantle after Wood et al., 1979) for the mafic Las Burras and Almagro rocks. Symbols are as in Figure 8. (B) Rare earth element (REE) patterns (normalized relative to chondrite, after McDonough and Sun, 1995) for the mafic Las Burras and Almagro rocks. The Chiar Kkollu and Leon Muerto basalts (Davidson and de Silva, 1995; Trumbull et al., 1999) are shown in A and B for comparison. (C, D) Chondrite-normalized REE patterns for Las Burras and Almagro rocks (normalized as in Fig. 10B). In the inset in Figure 10C the ranges in REE abundance for Las Burras and Almagro are compared.

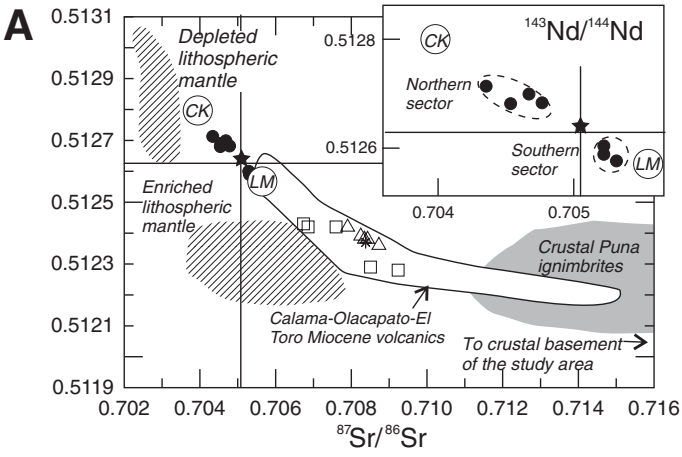

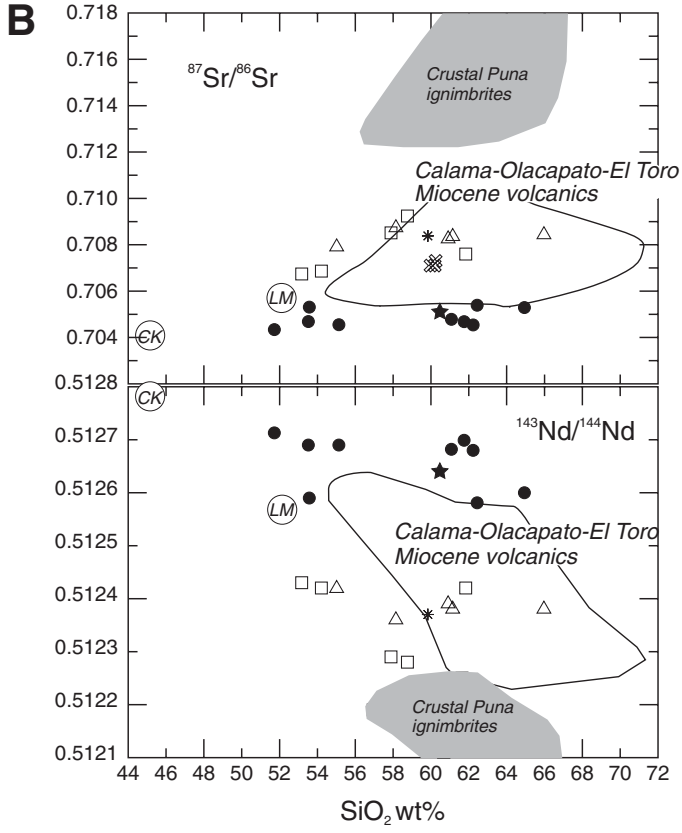

Figure 11. Sr versus Nd isotope ratio diagrams (A) and Sr and Nd isotope ratios versus silica (B). Symbols are as in Figure 8; open field: Calama–Olacapato–El Toro volcanic rocks from Matteini et al. (2002a, b) and Petrinovic et al. (2005). Dashed fields: lithospheric mantle domains from Lucassen et al. (2002, 2005); gray field: Puna crustal ignimbrites from Ort et al. (1996) and Francis et al. (1989). CK—Chiar Kkollu basalt, Davidson and de Silva (1995); LM—Leon Muerto basalt, Trumbull et al. (1999). Inset in A shows the isotopic difference between the northern and southern sectors of the Las Burras intrusion.

Blanquat, 1997; de Saint Blanquat et al., 1998). The magma would have been initially emplaced as a sill, developing into a laccolith as a result of prolonged injection. The uplift of the overburden, now partly eroded, accommodated the emplacement. The widespread strike-slip tectonics in the area are here interpreted as having been due to a local deviation in the pattern of overall ~E-W convergence (Cladouhos et al., 1994; Marrett et al., 1994; Marrett and Strecker, 2000; Acocella et al., 2007), which controlled the development of the thrust zones at the margins of the El Toro basin (Marrett et al., 1994; Marrett and Strecker, 2000, and references therein).

Almagro Volcanic Rocks

The Almagro volcanic units consist of several lava domes, lava flows, and scoria cones, related to monogenetic centers in a limited area (Fig. 12). Stratigraphic and geochronological data indicate that this volcanism occurred during ca. 13–6 Ma. Between ca. 13 Ma (the Puerta Tastil member) and 11 Ma (the Las Cuevas member) volcanism was lacking, whereas between ca. 8–6 Ma (the Lampazar and Almagro A, B, and C members) volcanism peaked in terms of frequency of eruptions, number of eruptive centers, volume of discharged magma, and spatial distribution of the products. After ca. 6 Ma, volcanism ceased in this part of the Eastern Cordillera. The Almagro volcanic activity produced small volumes of magma, and contrasts with the volcanism of the Calama–Olacapato–El Toro fault zone in the central-western Puna Plateau, where large stratovolcanoes were emplaced and large volumes of ignimbrites were erupted (Matteini et al., 2002b; Petrinovic et al., 2005).

The main directions of the feeder dikes are ~W-E, ~N-S, and ~WNW-ESE (Figs. 3 and 7). The dikes (1) are parallel or subparallel to the main N-S and NW-SE fault systems and (2) indicate extension along these trends, consistent with the structural data. Therefore, the volcanic activity with a peak at 8–6 Ma was probably related to the extensional episode along the Calama–Olacapato–El Toro fault zone.

El Toro Basin

The volcanic members interlayered with the Tertiary sediments of the El Toro basin help put stratigraphic and geochronological constraints on basin evolution during 11–6 Ma and its relationship with the Las Burras–Almagro Range (Fig. 12).

The amount and timing of uplift of the two N-S–trending ranges bordering the El Toro basin (the Las Burras–Almagro Range and the Sierra Pascha; Fig. 2) are quite different. The following stratigraphic, sedimentological, and structural evidence indicates that the Las Burras–Almagro Range was uplifted, eroded, and unroofed during 11–7 Ma:

1. The Agujas conglomerate (Marrett and Strecker, 2000) in the quebrada el Chorro and in the eastern part of the quebrada Carachi (sections 6 and 7 in Fig. 5) is younger than ca. 13 Ma (the Puerta Tastil member) and older than ca. 7 Ma (the Almagro A member). The clast composition of this conglomerate comprises, in order of abundance, quartzite and sandstone (from the Cambrian Meson Group), red granite, gray granodiorite and green porphyry (from the Precambrian Santa Rosa de Tastil batholith), and black siltstone (from the Puncoviscana Formation). This composition, together with the paleoflow direction reported by Hilley and Strecker (2005), suggests clast provenance from the Las Burras–Almagro Range.

2. The Las Cuevas member nonconformably overlies the Santa Rosa de Tastil batholith, suggesting that the southwesternmost part of the Las Burras–Almagro Range, which is close to the Calama–Olacapato–El Toro fault zone, was unroofed and exposed before ca. 11 Ma (Fig. 12).

3. The lower part of the Alfarcito conglomerate (Marrett and Strecker, 2000), cropping out in the quebrada Carachi, is younger than ca. 8 Ma (the Lampazar member) and older than ca. 7 Ma (the Almagro A member). The clasts are black siltstone (from the Puncoviscana Formation) and red granite (from the Precambrian Santa Rosa de Tastil batholith). This deposit thus records that at ca. 7 Ma the unroofing of the central Las Burras–Almagro Range reached the Puncoviscana cover.

4. In the Las Burras–Almagro Range the volcanic rocks of the Almagro A, B, and C members overlie the Puncoviscana Formation (Figs. 3, 5,

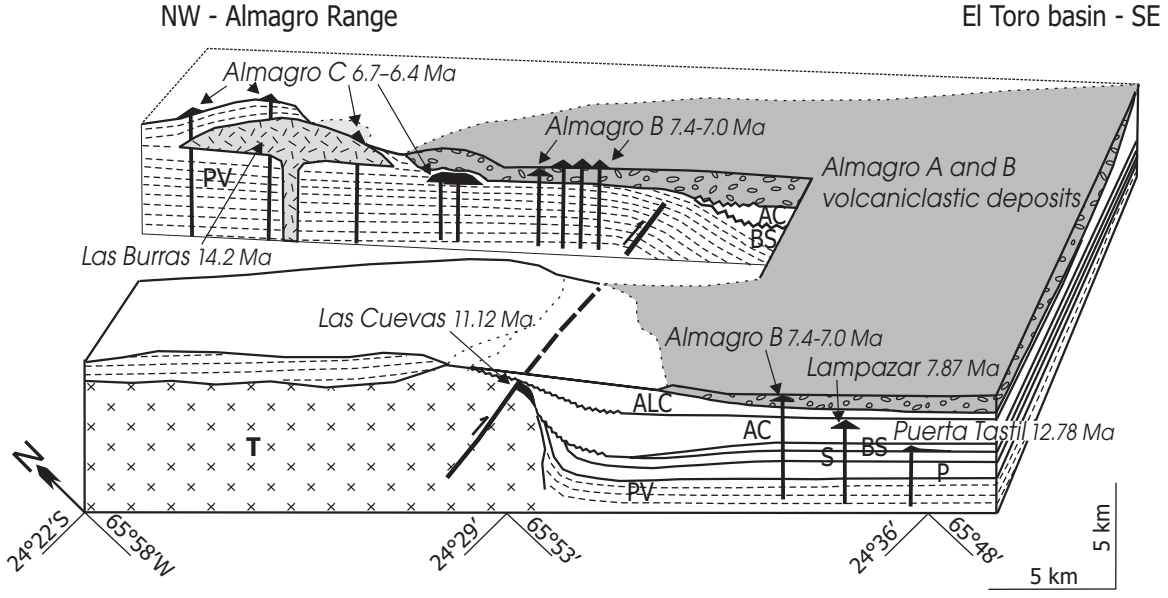

Figure 12. Schematic block diagram of the Las Burras–Almagro–El Toro region, illustrating the overall relationships between the Las Burras and Almagro magmatic activity and the evolution of the El Toro basin ca. 6 Ma (end of the Almagro volcanism). ALC—Alfarcito conglomerate; AC—Agujas conglomerate; BS—Barres sandstones; S—Salta Group; P—Paleozoic units; PV—Puncoviscana Formation; T—Santa Rosa de Tastil batholith.

and 6B) without the interposition of the continental clastic sequence exposed in the El Toro basin (Fig. 12). Therefore, these sedimentary deposits either were not deposited in this already uplifted area or were eroded before ca. 7 Ma.

5. The Las Burras pluton is directly overlain by the lava flows of the Almagro C member (Figs. 3 and 12), suggesting that the Puncoviscana Formation host sequence was eroded, and the intrusion exposed, before the onset of volcanism at 6–7 Ma.

The uplift of the Las Burras–Almagro Range is asymmetric because the structurally deepest unit, the Santa Rosa de Tastil batholith, is exposed in its southwestern part, and the younger units progressively crop out northward in stratigraphic order, from the Puncoviscana Formation to the Cambrian Meson Group, with an E-dipping regional tilt (Fig. 2). In the Las Burras–Almagro Range the original stratigraphic sequence over the Precambrian intrusive basement probably comprised the Puncoviscana Formation and the Paleozoic–Mesozoic units, and was eroded to form the Agujas conglomerate.

The Sierra Pascha retains the complete lithostratigraphic sequence, ranging from the Puncoviscana Formation to the Paleozoic–Mesozoic units (Fig. 2) and, hence, cannot have been the source area for the Agujas conglomerate. Following Hilley and Strecker (2005), we thus interpret that the Sierra Pascha was uplifted later than the Las Burras–Almagro Range, just after the end at ca. 6 Ma of the Las Burras–Almagro–El Toro volcanism. This confirms the overall eastward migration of deformation in this part of the Eastern Cordillera. Moreover, these data suggest that during and at the end of magmatic activity (ca. 6 Ma), the El Toro basin formed part of a continuous foreland basin (Fig. 12), extending eastward from the Las Burras–Almagro Range to the Salta area. The lithology and textures of the volcanic deposits of the Las Cuevas, Lampazar, and Almagro A members indicate interaction of magma with surface water and wet sediments (Table 3). The depositional environment of the El Toro basin was often lacustrine or water-saturated during a long period of time (11–7 Ma), producing peperites, magma-water contact facies at the margin of lava domes and lava flows, and autoclastic quenched lava flows (Table 3). During the uplift of the Las Burras–Almagro Range (11–7 Ma) the erosion rate, subsidence, and filling of the El Toro basin were probably close to equilibrium, and the relief remained negligible (Fig. 12).

Tectono-Magmatic Evolution

The data also provide constraints on the relations between tectonic structures and magmatism. The strike-slip faults active during the Miocene (Acocella et al., 2007) controlled the uplift of the Las Burras pluton at ca. 14 Ma. The peak of volcanism along the easternmost Calama–Olacapato–El Toro fault zone, during 11–6 Ma, was controlled by the extensional reactivation of the ~N-S– and ~NW-SE–striking strike-slip structures. The importance and extent of the extensional regime within an overall compressive context in the Eastern Cordillera are debated (Cladouhos et al., 1994; Marrett et al., 1994; Riller et al., 2001). It seems probable that the observed extension during 11–6 Ma was the result of orogen-parallel stretching upon reaching maximum orogen thickness (Riller et al., 2001). Since many thrust systems remained active during this period, the stretching episode must have been a local process. Finally, it is noteworthy that the easternmost Calama–Olacapato–El Toro fault zone was dominated in a the Miocene–Pliocene by significant differential vertical movements. Although the western sector of the area studied was dominated by uplift, leading to the exposure of Las Burras in few million years, the eastern sector underwent subsidence, with the formation of a continental basin (Fig. 12; Hilley and Strecker, 2005). However, because the eroded products of the western sector filled the basin to the east, the geologic evolution of the two areas was, in this period, closely correlated.

Magma Source Characteristics and Petrogenesis

The most mafic rocks in the Las Burras–Almagro–El Toro magmatic complex have Mg# of 63–75, are moderately fractionated, and have major element composition compatible with calc-alkaline suites. They fall in the field of intraplate rocks in La/Ta versus La/Yb diagrams (Fig. 13A), which utilize ratios of incompatible elements that are minimally involved in the initial steps of basalt fractionation. Accordingly, the Ba/Nb ratio is lower and Nb higher for these magmas than for the arc magmas, with similar

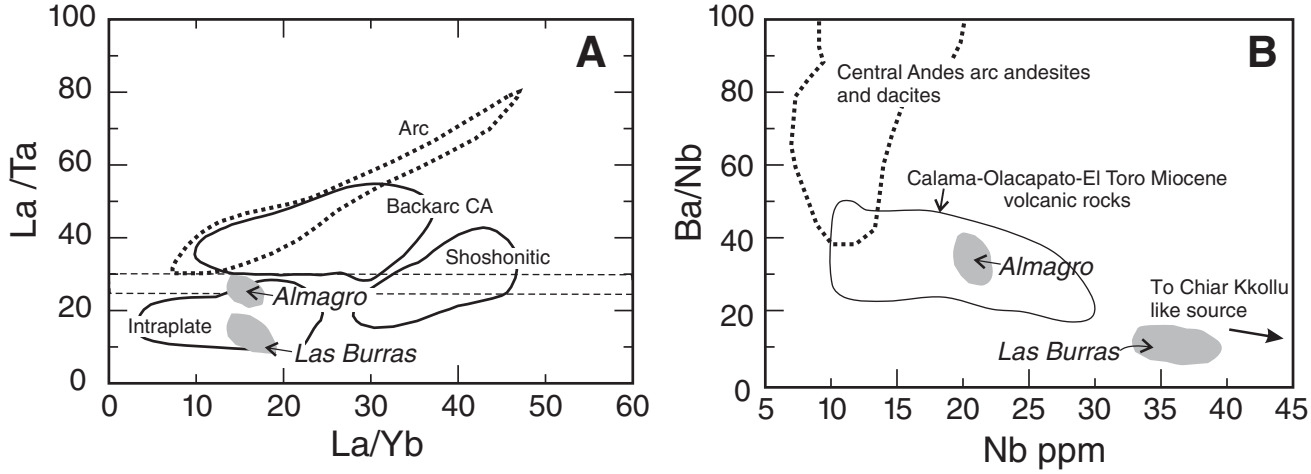

Figure 13. (A) La/Ta versus La/Yb, and (B) Ba/Nb versus Nb trace element diagrams for the mafic Las Burras–Almagro–El Toro rocks (gray fields). In A, the horizontal dashed lines indicate the bounding La/Ta ratio between intraplate and arc magmas. Fields for the Pliocene–Quaternary intraplate, shoshonitic, and backarc calc-alkaline Puna volcanism (Kay et al., 1994), the Miocene volcanic rocks erupted along the Calama–Olacapato–El Toro fault zone (Puntas Negras, Deruelle, 1994; Rincon, Quevar, Goddard et al., 1999; Tul Tul–Del Medio–Pocitos, Matteini et al., 2002a; Negra Muerta, Petrinovic et al., 2005), and the Central Volcanic Zone arc volcanic rocks (Thorpe et al., 1984; Trumbull et al., 1999) are reported for comparison. CA—calc-alkaline.

SiO_2 content, of the Central Andes (Fig. 13B). These characteristics recall the composition of the Chiar Kkollu basalt, which is a typical intraplate magma in the Central Andes (Davidson and de Silva, 1995).

Overall, the rocks of the Las Burras–Almagro–El Toro magmatic complex define two age groups: an older one emplaced between ca. 14 and ca. 13 Ma (the Las Burras and Puerta Tastil members) and a younger one erupted after ca. 11 Ma (the Las Cuevas, Lampazar, and Almagro members). These groups have markedly distinct Sr and Nd isotopic and trace element compositions (Figs. 11A and 14). Because isotopic ratios do not vary with the degree of melting and crystal fractionation, the variations in isotopic composition observed between and within the two phases must be ascribed to different mantle sources or to the intervention of crustal material, or both, and can be used to reveal the roles played by these processes in the genesis of the Las Burras–Almagro–El Toro magmas.

Magmatic Phase during 14–13 Ma

The primitive Sr and Nd isotope ratios of Las Burras and Puerta Tastil rocks (Table 4; Fig. 11A) are unusual among the arc and backarc Cenozoic rocks of the Central Andes, and approach the composition of depleted lithospheric mantle in this region, as inferred from mantle-derived Mesozoic peridotite xenoliths (Lucassen et al., 2002, 2005) and lavas (Kay et al. 1994). The Las Burras mafic rocks, with Mg# of 63 and rather low contents of Ni, Cr, and Co, have undergone some fractionation from their primary mantle melts. The development of the isotope composition of the Las Burras magma from a mantle-derived magma by interaction with crustal melts during crystal fractionation has been modeled by energy constrained–assimilation and fractional crystallization (EC-AFC) calculations (Spera and Bohrson 2001; Figure 15; model 1 in Table 5). For the purpose of these calculations, the Chiar Kkollu basalt was taken as near-primary magma of intraplate affinity, originated from the depleted upper mantle in this region. Regarding the crustal source, the involvement of the Paleozoic basement was tested in the calculations using a granitoid sample from Becchio et al. (1999) and average values from Becchio et al. (1999) and Lucassen et al. (1999, 2001). The middle-lower crust in the region directly north of Las Burras–Almagro–El Toro is considered to be predominantly felsic (Zandt et al., 1994; Beck et al., 1996; Swenson et al., 2000; Beck and Zandt, 2002). However, as the existence of mafic compositions in the crust under the El Toro region cannot be excluded, a mafic lower crust contribution was tested, using the composition of xenoliths from the Cretaceous magmatism of the Central Rift of NW Argentina (Lucassen et al., 1999). The results of EC-AFC modeling (Table 5) indicate a moderate involvement of Paleozoic basement-like crustal material (assimilated mass/crystallized mass ~0.26).

The abundance of elements such as Rb and K (Table 4) in the Las Burras intrusion could not be obtained by calculations involving contamination by upper crustal material. In particular, the Rb and K_2O contents, and the K_2O/Na_2O and $K_2O + Na_2O$ values of Las Burras rocks are high, close to those of Pliocene–Quaternary intraplate and shoshonitic backarc mafic rocks (Kay et al., 1994). We can exclude the possibility that analytical problems affect the compositions reported in Table 4 (see Appendix). The possibility that these values are markedly affected by alteration by K-Rb–bearing minerals can also be excluded on the basis of the petrographic evidence and on the fact that the values for loss on ignition (L.O.I.; Table 4) are generally low and do not correlate with the K_2O values. Therefore, the high K and Rb are a characteristic of Las Burras rocks.

The isotope ratios of Las Burras rocks (see inset in Fig. 11A) indicate two groups of rocks, corresponding to the southern feeder zone and the central northern sector of the outcropping intrusion. Within each group a considerable variation of major element contents is observed, with nearly constant isotopic composition (Fig. 11B). The variation in Sr and Nd isotope ratios between these two groups can be modeled by assimilation of crustal material (model 2 in Table 5; assimilated mass/crystallized mass ~0.47), which probably occurred before magma emplacement, during its rise through the crust. The range of composition within each group, leaving the Sr and Nd isotope ratios unaffected, can thus be ascribed to shallow differentiation, possibly during pluton emplacement.

Magmatic Phase during 11–6 Ma

The most primitive Almagro volcanic rocks are basaltic andesites with K_2O content, and K_2O/Na_2O and large ion lithophile element/high field strength element (LILE/HFSE) values intermediate between the Las Burras magmas and those of the Central Andes arc at a similar degree of evolution (Figs. 10A and 13). High-temperature minerals generated by early crystallization of mantle-derived magmas are present, such as Mg-rich olivine, Cr-spinel, and diopside (Table DR3; see footnote 1). The AlIV- and Ti-rich and Si-poor character of diopside is similar to that of alkaline basalts (Fig. DR1; see footnote 1). The pyroxenite enclaves display Mg- and Cr-poor minerals with respect to the basaltic association and are interpreted as deep mafic cumulates (Gioncada et al., 2006).

The higher $^{87}Sr/^{86}Sr$ and lower $^{143}Nd/^{144}Nd$ ratios of the Almagro basaltic andesites with Mg# 71–75, in comparison with Las Burras mafic rocks with Mg# 63 (Figs. 11A and 11B), are striking features of the Las Burras–Almagro–El Toro complex. The strong similarities in trace

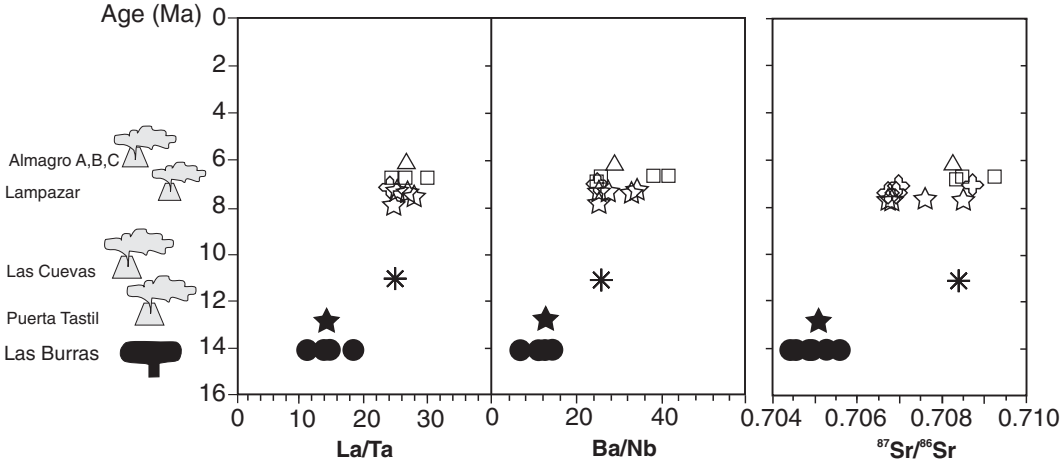

Figure 14. La/Ta, Ba/Nb, and $^{87}Sr/^{86}Sr$ ratios versus ages for the Las Burras–Almagro–El Toro magmatic complex (symbols as in Fig. 8). Note the change of magma chemistry with time for the different magmatic pulses in the history of the Las Burras–Almagro–El Toro magmatism. Note also that the change in the reported trace element ratios is independent of the degree of differentiation of the rocks.

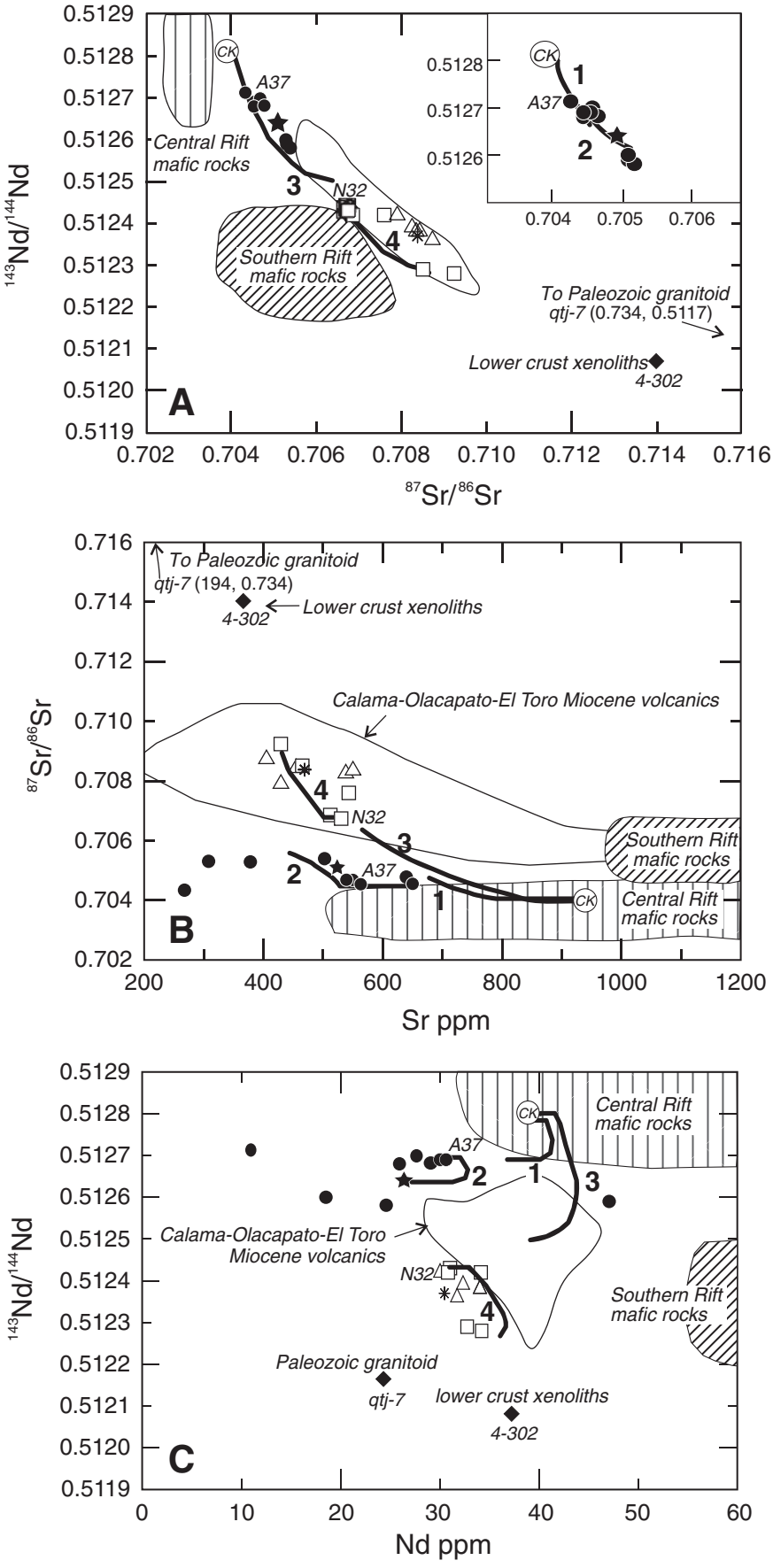

Figure 15. Plots of $^{143}Nd/^{144}Nd$ versus $^{87}Sr/^{86}Sr$ (A), $^{87}Sr/^{86}Sr$ versus Sr (B), and $^{143}Nd/^{144}Nd$ versus Nd (C) for Las Burras–Almagro–El Toro rocks (symbols as in Fig. 8) in comparison with the fields for the Calama–Olacapato–El Toro Miocene volcanics (open field, Deruelle, 1994; Goddard et al., 1999; Matteini et al., 2002a; Petrinovic et al., 2005), and the Central Rift and Southern Rift mafic rocks and xenoliths (Lucassen et al., 2002, 2005). Heavy lines represent energy constrained–assimilation and fractional crystallization (EC-AFC) models, to test the derivation of Las Burras (sample A37) and Almagro (sample N32) rocks from Chiar Kkollu-like (CK) parent magma (lines 1 and 3), and the compositional ranges within the rocks of the 14–12 and the 11–6 Ma magmatic phases (lines 2 and 4). See text for explanation and Table 5 for compositional and thermal parameters for the EC-AFC calculations.

TABLE 5. ENERGY CONSTRAINED–ASSIMILATION AND FRACTIONAL CRYSTALLIZATION (EC-AFC) MODELS

EC-AFC models in Figure 14	1	2	3	4
Compositional parameters				
Sr parent magma (ppm)	936	650	936	530
Sr contaminant (ppm)	194	194	353	194
$^{87}Sr/^{86}Sr$ parent magma	0.70405	0.70455	0.70405	0.70674
$^{87}Sr/^{86}Sr$ contaminant	0.734	0.734	0.714	0.734
Nd parent magma (ppm)	40	30	40	31
Nd contaminant (ppm)	23	23	38	23
$^{143}Nd/^{144}Nd$ parent magma	0.5128	0.51269	0.5128	0.51243
$^{143}Nd/^{144}Nd$ contaminant	0.51219	0.51219	0.51209	0.51219
D_{Sr} crystallization	1.5	1.5	1.9	1.2
D_{Sr} melting	1	1.2	0.1	1.5
D_{Nd} crystallization	0.5	0.5	0.6	0.5
D_{Nd} melting	0.5	0.25	0.15	0.4
Thermal parameters				
$T_{liquidus}$ parent magma °C	1210	1130	1210	1190
T_0 parent magma °C	1210	1130	1210	1190
$T_{liquidus}$ crust °C	1000	1000	1100	1100
T_0 crust °C	300	300	650	600
$T_{solidus}$ crust °C	900	900	850	950
cpm J/kg K	1484	1484	1529	1484
cpa J/kg K	1388	1388	1370	1388
hcry J/kg	396000	396000	396000	396000
hfus J/kg	354000	354000	270000	354000
Ma*	0.08	0.14	0.15	0.18
Mc	0.30	0.3	0.30	0.46

Note: Model 1: test for the differentiation of a Chiar Kkollu–like basalt with assimilation of Paleozoic crust.

Model 2: differentiation of a Las Burras–like basalt with assimilation of Paleozoic crust (Becchio et al., 1999).

Model 3: differentiation of a Chiar Kkollu–like basalt with assimilation of lower crust (Lucassen et al., 1999).

Model 4: differentiation of an Almagro-like basalt with assimilation of Paleozoic crust.

Ma*: assimilated mass/crystallized mass.

Thermal parameters from Bohrson and Spera (2001). Mineral KD from Luhr and Carmichael (1980) and Bacon and Druitt (1988).

element patterns of the mafic rocks (Figs. 10A and 10B) could suggest a mantle source for the Almagro rocks similar to the depleted mantle generating Las Burras magmas. The Almagro isotopic composition thus would require a major contribution of continental crust. Derivation of the Almagro magmas from a mantle-derived parent was thus modeled as an EC-AFC process (model 3 in Table 5), using the same end members as for the Las Burras calculations. The results show that too much fractionation is required in comparison with likely assimilation of highly radiogenic upper crust material (assimilated mass/crystallized mass ~1); this is contrary to the mafic nature of the Almagro basaltic andesite. Intervention of hot, mafic lower crust would be required to model the geochemical features of Almagro rocks, starting from a depleted mantle source (Table 5).

A derivation of the primitive Almagro magmas from the enriched subcontinental lithospheric mantle domain represented by the mafic rocks and xenoliths from the Paranà and the Cretaceous Southern Rift of NW Argentina (Fig. 11A; Lucassen et al., 2002, 2005) is instead unlikely because their composition does not fit with the Almagro Sr and Nd isotopic trend (Fig. 15).

Thus, in a first hypothesis, the possibility exists that the Almagro magmas were derived from a depleted mantle source such as Las Burras, modified by the intervention of a mafic crustal component. Alternatively, the enriched isotopic composition was a characteristic of the primary Almagro magmas, related to the presence of heterogeneities in the lithospheric mantle in this region. In our opinion, taking into account the scarce evidence of mafic components in the crust in this region and the possible presence of heterogeneities in the mantle, the latter hypothesis is to be preferred. Lucassen et al. (2002) describe rare mafic rocks from the Cretaceous Central Rift magmatism of NW Argentina, with anomalously enriched compositions.

The range in isotopic ratios of the Almagro volcanic rocks suggests crustal contamination during magma differentiation (Fig. 11A). However, the lack of correlation of the isotopic ratios with silica (Fig. 11B) or with stratigraphic position indicates instead that the volcanic members are related to magma batches with independent evolutionary histories. To illustrate this, model 4 represents EC-AFC evolution within the rocks of the Almagro B member, starting from basaltic andesite (Table 5; Fig. 15).

Geodynamic Model

The geological and petrological data concerning the magmatism in the easternmost Calama–Olacapato–El Toro complex shed some light on the evolution of this part of the Central Andes between 14 and 6 Ma, suggesting the geological model in Figure 16.

During the early–middle Miocene a thin lithosphere characterized the Central Andes at this latitude, and the generation of magmas was probably controlled by steepening of the formerly almost flat slab (Isacks, 1988; Kay et al., 1999; Kay and Mpodozis, 2001). Partial melting of the depleted lithospheric mantle generated the Las Burras–type magmas between 14 and 13 Ma (Fig. 16A). The low Sr and high Nd isotopic ratios and the magmatic evolution of the Las Burras rocks suggest a moderate involvement of the Paleozoic basement during magma ascent, with fractional crystallization and negligible crustal contamination after pluton emplacement.

Between ca. 13 and ca. 11 Ma, volcanic activity was absent (Fig. 14), as the Puerta Tastil lavas at ca. 13 Ma are overlain by a succession of sedimentary rocks (Agujas conglomerate) devoid of volcanic clasts. This lack of volcanism could relate to the compression, shortening, and crustal thickening that affected this portion of the Central Andes during the late Miocene (Cladouhos et al., 1994; Marrett et al., 1994; Marrett and Strecker, 2000; Reynolds et al., 2000; Coutand et al., 2001; Riller et al., 2001; Muller et al., 2002). Underthrusting of the Brazilian Shield could have contributed to this lithospheric thickening at the Eastern Cordillera–Puna boundary (Fig. 16B), as was pointed out by Isacks (1988), Beck and Zandt (2002), and Babeyko and Sobolev (2005). Beck and Zandt (2002) deduced underthrusting of the Brazilian Shield lithosphere under the Andean structure at ~21°S, using geophysical data, and extrapolated this process to 23°S.

From ca. 11 Ma on, volcanism was active in the region until 6 Ma (Figs. 14 and 16C), and the magmas reached the surface through ~NW-SE– and ~N-S–trending strike-slip structures, possibly reactivated as extensional systems. During 11–6 Ma, the evolution of the El Toro basin was complex: its western part was affected by rapid uplift, whereas its eastern part underwent subsidence. The rapid uplift and erosion of the La Burras–Almagro Range is evidenced by the emplacement of the ca. 6 Ma Almagro lavas directly on the exposed Las Burras intrusion.

At 11 Ma the geochemical characteristics of the mantle-derived magmas changed significantly. This abrupt change could suggest the occurrence of partial melting of different

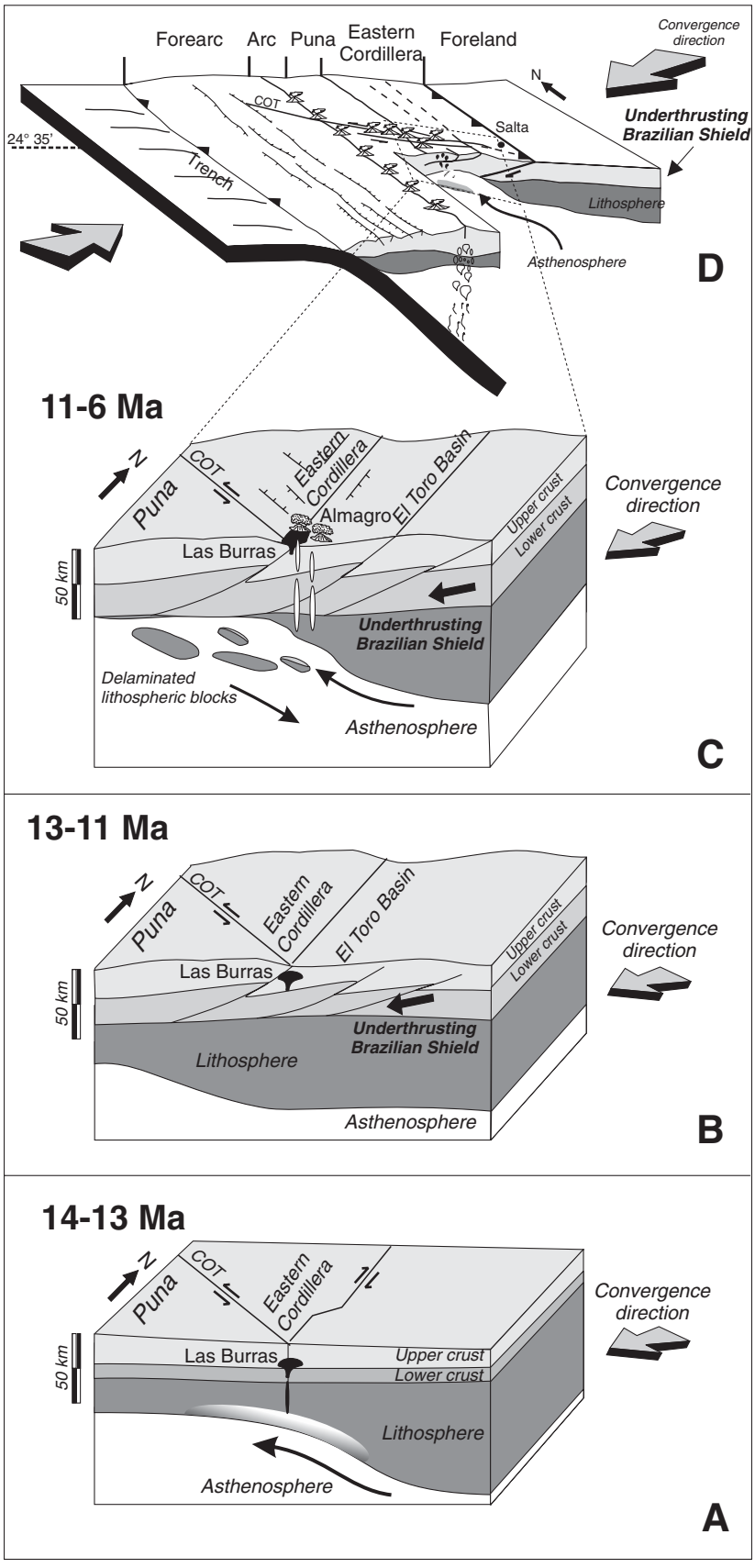

Figure 16. Evolution of the Puna–Eastern Cordillera boundary, at 24°35′S, during the middle–late Miocene. (A) During 14–13 Ma, lithospheric thinning caused partial melting of the lithospheric mantle. Strike-slip tectonics controlled the ascent of mantle-derived magmas and their shallow emplacement. (B) During 13–11 Ma, underthrusting of the Brazilian Shield contributed to a significant thickening of the lithosphere beneath the Eastern Cordillera. In this time span, volcanic activity was rare or absent. (C) During 11–6 Ma, the lithospheric thickening caused delamination under the Eastern Cordillera. This facilitated the upflow of asthenosphere, leading to partial melting of different lithospheric mantle and crustal domains. (D) La Burras–Almagro–El Toro magmatic complex during the late Miocene, given the convergence regime between the Nazca plate and the South American margin. COT—Calama–Olacapato–El Toro fault system.

lithospheric mantle and crustal material with respect to the previous phase. This may be explained by lithospheric delamination beneath the Central Andes, as proposed by several workers (Kay and Kay, 1993; Beck and Zandt, 2002; Yuan et al., 2002). The crustal shortening, thickening, and underthrusting of the Brazilian Shield could have induced the detachment of lithospheric blocks, leading to a piecemeal delamination process (Coira and Kay, 1993; Kay et al., 1994; Beck and Zandt, 2002; McQuarrie et al., 2005). The removal of mantle lithosphere and consequent upflow of asthenosphere thus may have created the conditions for partial melting of different lithospheric domains (Figs. 16C and 16D). West of the Las Burras–Almagro–El Toro region, in the Puna Plateau, delamination is thought to have been responsible for widespread crustal melting, causing large silicic ignimbrite eruptions in the late Miocene and Pliocene (Coira and Kay, 1993; Kay et al., 1994; de Silva et al., 2006). The small volume and mafic character of the Almagro volcanism suggest that the magma generation at the Eastern Cordillera–Puna boundary occurred at the margin of this thermally anomalous region (Fig. 16C).

Role of Calama–Olacapato–El Toro Fault Zone in Las Burras–Almagro–El Toro Magmatism

The effect of the Calama–Olacapato–El Toro fault zone in the ascent of magmas appears to have been limited during the initial strike-slip event, when the Las Burras intrusion was emplaced. The emplacement of this intrusion seems to have been largely controlled by ~N-S–trending dextral structures related to the buildup of the Eastern Cordillera. However, the intrusion lies along the easternmost part of the Calama–Olacapato–El Toro fault zone in an area characterized by widespread NW-SE–trending strike-slip (older event) and extensional (more recent event) structures (Fig. 7). It is therefore possible that, even though not directly controlling the emplacement of the intrusion, the Calama–Olacapato–El Toro structures controlled the rise of magma at a more general scale, providing, through fracturing, preferred paths for magma ascent through the crust and inducing local decompression. It is thus possible that the N-S–striking structures are responsible only for the final rise and emplacement of magma while, at deeper crustal levels, the WNW-ESE Calama–Olacapato–El Toro parallel structures could have controlled the activation of the magma ascent paths. Conversely, the role of the Calama–Olacapato–El Toro fault zone in the rise and emplacement of the magmas between 11 and 6 Ma is more evident. The dominant process acting along the Calama–Olacapato–El Toro fault zone was extensional, and for this period there is widespread evidence of extrusion along WNW-ESE extensional structures.

In summary, different structures were active at different structural levels during the rise and emplacement of the intrusion, while the rise and emplacement of magmas feeding the younger volcanic activity were closely controlled by structures associated with the Calama–Olacapato–El Toro fault zone.

CONCLUSIONS

Study of the Las Burras–Almagro–El Toro magmatic complex results in the following conclusions regarding the evolution of the Eastern Cordillera of the Central Andes at 24°S.

1. The Las Burras–Almagro–El Toro magmatic complex consists of intrusive and volcanic rocks emplaced between 14 and 6 Ma along the easternmost Calama–Olacapato–El Toro fault zone. These ages span all the magmatic activity along the Calama–Olacapato–El Toro lineament (Matteini et al., 2002a, 2002b; Petrinovic et al., 2005).

2. The Las Burras pluton has a laccolith shape and was probably emplaced along a releasing bend created by the activity of N-S–trending dextral faults in an overall context of compression. The Calama–Olacapato–El Toro fault zone had limited control on the rise and emplacement of the Las Burras magmas. In contrast, the fault zone appears to have closely controlled the emplacement of the subsequent Almagro volcanic rocks, which are associated with WNW-ESE–trending extensional systems and were mostly erupted along ~NW-SE– and ~N-S–trending strike-slip structures, possibly reactivated as extensional systems.

3. The Las Burras–Almagro–El Toro magmatism, despite its calc-alkaline major element signature, shows trace element composition, suggesting intraplate characteristics, and hence it cannot be considered directly linked to the subduction of the Nazca plate under the South American margin.

4. The Las Burras intrusion and the ca. 13 Ma lavas show the isotopic composition of a lithospheric depleted mantle similar to that deduced from the composition of mantle xenoliths in nearby Cretaceous volcanic rocks (Lucassen et al., 2002, 2005). The younger (11–6 Ma) Almagro volcanic group lavas could have originated from partial melting of lithospheric mantle domains with distinct isotopic characteristics from the Las Burras source.

5. In the regional context we speculate that the change in magma composition at 11 Ma was linked to delamination following the thickening of the continental lithosphere and the possible underthrusting of the Brazilian Shield. Delamination caused the uprise of asthenosphere and melting of part of the overlying lithosphere. This process had its greatest effects in the Puna Plateau, resulting in huge ignimbrite sheets, while at the Puna Plateau–Eastern Cordillera boundary, at the margin of the extensive thermally anomalous zone, it led to the rise of small volumes of mainly mafic magmas.

APPENDIX: ANALYTICAL METHODS

Major and minor element analyses of minerals were performed on polished rock sections at CNR-IGG, Firenze, Italy, using a JEOL JXA-8600 electron microprobe equipped with four WDS spectrometers integrated with an EDS system. Accelerating voltage and beam current were 15 kV and 10 nA, respectively, with variable counting times. During analysis of feldspars a defocused beam was used to minimize alkali loss under the beam. The data were corrected using the Bence and Albee (1968) method. Standard deviations were <3% for most major elements and 5% for trace elements (Vaggelli et al., 1999). Other analyses were carried out with a Philips XL30 scanning electron microscope equipped with microanalysis EDAX (standard-less software DXi4) at the Dipartimento di Scienze della Terra, Università di Pisa, Italy (acceleration voltage 20 kV, beam current 5 nA, live time 100 s). The accuracy is better than 0.5% if abundance is >15 wt%, is 1% if abundance is ~5 wt%, and is better than 20% if abundance is ~0.5 wt%.

XRF analysis was done at the Dipartimento di Scienze della Terra, Università di Pisa, Italy. Whole-rock analyses of major oxides were done on fused samples with an ARL 9400 XPp instrument. Major and trace elements were analyzed on powdered whole-rock samples with a Philips PW 1480 instrument. The concentrations were calculated, correcting for matrix effects following the method of Franzini et al. (1975). Accuracy was monitored using international standards and is better than 10% for concentrations higher than 10 ppm. Using inductively-coupled-plasma mass spectroscopy (ICP-MS) (VG PQII Plus), analysis was carried out on a selection of samples, allowing the determination of a wide set of trace elements, with accuracy to within ±5%.

Rb-Sr analyses were carried out on ~100 mg of whole-rock powders and mineral separates. Samples were dissolved into Savillex screw-top beakers using a mixture of HF and HNO_3. One aliquot was spiked using a mixed ^{87}Rb-^{84}Sr spike solution. Rb and Sr were separated using standard separation techniques. Total Rb and Sr procedural blanks were lower than 1 and 0.25 ng, respectively. An uncertainty of 1% was assigned to the Rb/Sr ratio on the basis of replicate analyses of natural samples. Rb and Sr isotopic analyses were determined using a VG Isomass 54E mass spectrometer (at IGG, CNR Pisa, Italy). At the time of data collection the NIST SRM 987 yielded an average of 0.710240 ± 0.000016 (2σ), which was assumed to be the minimum uncertainty in isochron calculations. Isochrons were calculated using the Isoplot/Ex program, v. 3.00 (Ludwig, 2003).

Whole-rock Sr and Nd isotopic analyses were determined using a Finnigan MAT 262V multicollector mass spectrometer (at IGG, CNR Pisa, Italy). After use of conventional ion-exchange procedures for Sr and Nd separation from the matrix, the Sr total blank was <2 ng, whereas the Nd total blank was <1 ng during the period of measurements. Measured

$^{87}Sr/^{86}Sr$ ratios were normalized to $^{86}Sr/^{88}Sr = 0.1194$, and $^{143}Nd/^{144}Nd$ ratios to $^{146}Nd/^{144}Nd = 0.7219$. During the collection of isotopic data, 15 replicate analysis of the NIST SRM 987 ($SrCO_3$) standard gave an average value of 0.710241 ± 12 (2σ), and 14 measures of La Jolla gave an average $^{143}Nd/^{144}Nd$ of 0.511851 ± 7 (2σ). All $^{87}Sr/^{86}Sr$ data were normalized to a value of 0.71025 for the NIST SRM 987 standard.

Argon isotope analyses were carried out at LSCE, Gif-sur-Yvette, France. The isotopic composition and abundance of Ar were determined using an unspiked technique described by Charbit et al. (1998). This technique differs from the conventional isotope dilution method in that argon extracted from the sample is measured in sequence with purified aliquots of atmospheric argon at the same working gas pressure in the mass spectrometer. This allows suppression of mass discrimination effects between the atmospheric reference and the unknown, and allows quantities of radiogenic $^{40}Ar^*$ as small as 0.14% to be detected on a single-run basis (Scaillet and Guillou, 2004). The mass spectrometer sensitivity was 5.7×10^{-3} mol/A @ m/e = 40 with amplifier backgrounds of 75×10^{-12} A ≅ m/e = 40 (10^9 ohm resistor), and $5.75\ 10^{-14}$ A @ m/e = 36 (10^{11} ohm resistor). Groundmass from fresh samples was prepared following the methods of Guillou et al. (1998). Values of loss on ignition show that the dated samples are unaltered. Phenocrysts and xenocrysts, which are potential carriers of extraneous ^{40}Ar (including excess and inherited components), were eliminated using magnetic, gravimetric, and visual hand picking separation. Replicate unspiked K-Ar age determinations were done on the microcrystalline groundmass of samples. The determination of K was carried out by atomic spectrophotometry with a relative precision of 1%. Argon was extracted by radio frequency heating of 0.6–1.0 g of sample, then transferred to an ultrahigh-vacuum glass line and purified with a titanium sponge and Zr-Ar getters. Isotopic analyses were performed on total ^{40}Ar contents ranging between 5×10^{-11} and 2×10^{-10} moles using a 180°, 6-cm-radius mass spectrometer with an accelerating potential of 620 v. The spectrometer was operated in static mode, but its volume was varied to give equal ^{40}Ar signals for the air aliquots and the samples. Beam sizes were measured simultaneously on a double Faraday collector in sets of 100 online acquisitions with a 1 s integration time. The atmospheric correction is monitored via measurements of atmospheric argon for each individual sample. The manometric calibration of the mass spectrometer was based on periodic, replicate determinations of international dating standards of known K-Ar age using the same procedure for the unknowns, as described by Charbit et al. (1998). This allows the total ^{40}Ar content of the sample to be determined with a precision of about ±0.2% (2σ). Standards used include LP-6 (127.8 ± 0.7 Ma; Odin, 1982) and HD-B1 (24.21 ± 0.32 Ma; Fuhrman et al., 1987; Hess and Lippolt, 1994; Hautmann and Lippolt, 2000). At the 95% confidence level, the values adopted here are consistent with those obtained for several $^{40}Ar/^{39}Ar$ standards through the intercalibration against biotite GA-1550 by Renne et al. (1998) and Spell and McDougall (2003). Uncertainties for the K and Ar data are 1σ analytical only and consist of propagated and quadratically averaged experimental uncertainties arising from the K, ^{40}Ar (total), and $^{40}Ar^*$ determinations. Uncertainties of the ages are given at 2σ.

ACKNOWLEDGMENTS

This work was carried out with financial support of the Italian Ministry of University and Research (PRIN Project 2003-2005) and in the framework of the scientific convention between Pisa and Salta Universities (Projects PID CONICET N° 5341 and CIUNSA 20/D-249, Salta University, Argentina). Constructive and helpful reviews by S.M. Kay and F. Lucassen significantly improved the paper, which also greatly benefited by the thoughtful comments of N. Riggs. We are indebted to Rob Westaway for polishing the English style.

REFERENCES CITED

Acocella V., Vezzoli L., Omarini R., Matteini M., and Mazzuoli R., 2007, Kinematic variations across Eastern Cordillera at 24°S (Central Andes): Tectonic and magmatic implications: Tectonophysics, doi: 10,1016/j.tecto.2007.02.001.

Allmendinger, R.W., Ramos, V., Jordan, T., Palma, M., and Isacks, B., 1983, Paleogeography and Andean structural geometry, Northwestern Argentina: Tectonics, v. 2, p. 1–16, doi: 10.1029/TC002i001p00001.

Babeyko, A.Y., and Sobolev, S.V., 2005, Quantifying different modes of the late Cenozoic shortening in the central Andes: Geology, v. 33, p. 621–624, doi: 10.1130/G21126.1.

Bacon, C.R., 1986, Magmatic inclusions in silicic and intermediate volcanic rocks: Journal of Geophysical Research, v. 91, p. 6091–6112, doi: 10.1029/JB091iB06p06091.

Bacon, C.R., and Druitt, T.H., 1988, Compositional evolution of the zoned calcalkaline magma chamber of Mount Mazama, Crater Lake, Oregon: Contributions to Mineralogy and Petrology, v. 98, p. 224–256, doi: 10.1007/BF00402114.

Becchio, R., Lucassen, F., Franz, G., Viramonte, J., and Wemmer, K., 1999, El basamento paleozoico inferior del noroeste de Argentina (23°–27°S), metamorfismo y geocronologia, *in* Bonorino, R., et al., eds., Geologia del Noroeste Argentino: Salta, Argentina, Relatorio, Congreso Geológico Argentino, 14th, p. 58–72.

Beck, S.L., and Zandt, G., 2002, The nature of orogenic crust in the central Andes: Journal of Geophysical Research, v. 107, doi: 10,1029/2000JB000124.

Beck, S.L., Zandt, G., Myers, S.C., Wallace, T.C., Silver, P.G., and Drake, L., 1996, Crustal thickness variations in the central Andes: Geology, v. 24, p. 407–410, doi: 10.1130/0091-7613(1996)024<0407:CTVITC>2.3.CO;2.

Bence, A.E., and Albee, A.L., 1968, Empirical correction factors for the electron microanalysis of silicates and oxides: Journal of Geology, v. 76, p. 382–403.

Bohrson, W.A., and Spera, F.J., 2001, Energy-constrained open-system magmatic processes II: Application of energy-constrained assimilation fractional crystallization (EC-AFC) model to magmatic systems: Journal of Petrology, v. 42, p. 1019–1041, doi: 10.1093/petrology/42.5.1019.

Busby-Spera, C.J., and Saleeby, J.B., 1990, Intra-arc strike-slip fault exposed at batholithic levels in the Southern Sierra Nevada, California: Geology, v. 18, p. 255–259, doi: 10.1130/0091-7613(1990)018<0255:IASSFE>2.3.CO;2.

Cabrera, J., Sebrier, M., and Mercier, J.L., 1987, Active normal faulting in high plateaus of Central Andes: The Cuzco region (Peru): Annales Tectonicae, v. 1, p. 116–138.

Charbit, S., Guillou, H., and Turpin, L., 1998, Cross calibration of K-Ar standard minerals using an unspiked Ar measurement technique: Chemical Geology, v. 150, p. 147–159, doi: 10.1016/S0009-2541(98)00049-7.

Cladouhos, T.T., Allmendinger, R.W., Coira, B., and Farrar, E., 1994, Late Cenozoic deformation in the Central Andes: Fault kinematics from the northern Puna, northwestern Argentina and southwestern Bolivia: Journal of South American Earth Sciences, v. 7, p. 209–228, doi: 10.1016/0895-9811(94)90008-6.

Coira, B., and Kay, S.M., 1993, Implications of Quaternary volcanism at Cerro Tuzgle for crustal and mantle evolution of the Puna Plateau, central Andes, Argentina: Contributions to Mineralogy and Petrology, v. 113, p. 40–58, doi: 10.1007/BF00320830.

Coira, B., Kay, S.M., and Viramonte, J., 1993, Upper Cenozoic magmatic evolution of the Argentine Puna—A model for changing subduction geometry: International Geology Review, v. 35, p. 677–720.

Coombs, M.L., and Gardner, J.E., 2004, Reaction rim growth on olivine in silicic melts: Implications for magma mixing: American Mineralogist, v. 89, p. 748–758.

Coombs, M.L., Eichelberger, J.C., and Rutherford, M.J., 2003, Experimental and textural constraints on mafic enclave formation in volcanic rocks: Journal of Volcanology and Geothermal Research, v. 119, p. 125–144, doi: 10.1016/S0377-0273(02)00309-8.

Coutand, I., Cobbold, P.R., de Urreiztieta, M., Gautier, P., Chauvin, A., Gapais, D., Rossello, E.A., and Lopez-Gamundi, O., 2001, Style and history of Andean deformation, Puna plateau, northwestern Argentina: Tectonics, v. 20, p. 210–234, doi: 10.1029/2000TC900031.

Davidson, J.P., and de Silva, S.L., 1995, Late Cenozoic magmatism of the Bolivian Altiplano: Contributions to Mineralogy and Petrology, v. 119, p. 387–408.

Deruelle, B., 1994, Petrology of Quaternary shoshonitic lavas of Northwestern Argentina, *in* Harmon, R.S., and Rapela, C.W., eds., Andean magmatism and its tectonic setting: Geological Society of America Special Paper 265, p. 201–217.

de Saint Blanquat, M., Tikoff, B., Teyssier, C., and Vigneresse, J.L., 1998, Transpressional kinematics and magmatic arcs, *in* Holdsworth, R.E., et al., eds., Continental transpressional and transtensional tectonics: Geological Society of London Special Publication 135, p. 327–340.

de Silva, S.L., Zandt, G., Trumbull, R., and Viramonte, J., 2006, Large scale silicic volcanism: The result of thermal maturation of the crust, *in* Chen Yun-tai, ed., Advances in geosciences: River Edge, New Jersey, World Scientific Press, Proceedings of the Asia-Oceania Geosciences Society, p. 215–230.

Dewey, J.F., and Lamb, S.H., 1992, Active tectonics of the Andes: Tectonophysics, v. 205, p. 79–95, doi: 10.1016/0040-1951(92)90419-7.

Dietl, C., and Koyi, H.A., 2002, Emplacement of nested diapirs: Result of centrifuge modelling, *in* Schellart, W.P., and Passchier, C., eds., Analogue Modelling of Large-Scale Tectonic Processes: Journal of the Virtual Explorer, v. 6, p. 81–88.

Drozdzewski, G., and Mon, R., 1999, Oppositely-verging thrusting structures in the North Argentine Andes compared with German Variscides: Acta Geologica Hispanica, v. 34, p. 185–197.

Ebinger, C.J., and Casey, M., 2001, Continental breakup in magmatic provinces: An Ethiopian example: Geology, v. 29, p. 527–530, doi: 10.1130/0091-7613(2001)029<0527:CBIMPA>2.0.CO;2.

Ferré, E.C., Bordarier, C., and Marsh, J.S., 2002, Magma flow inferred from AMS fabrics in a layered mafic sill, Insizwa, South Africa: Tectonophysics, v. 354, p. 1–23, doi: 10.1016/S0040-1951(02)00273-1.

Francis, P.W., Sparks, S.J., Hawkesworth, C.J., Thorpe, R.S., Pyle, D.M., Tait, S.R., Mantovani, M.S., and McDermott, F., 1989, Petrology and geochemistry of volcanic rocks of the Cerro Galan caldera, northwestern Argentina: Geological Magazine, v. 126, p. 515–547.

Franzini, M., Leoni, L., and Saitta, M., 1975, Revisione di una metodologia analitica per fluorescenza X, basata sulla correzione complete degli effetti di matrice: Società Italiana di Mineralogia e Petrografia, v. 31, p. 365–378.

Fuhrman, U., Lippolt, H., and Hess, J.C., 1987, HD-B1 Biotite reference material for K-Ar chronometry: Chemical Geology, v. 66, p. 41–51.

Giese, P., Scheuber, E., Schilling, F., Schmitz, M., and Wigger, P., 1999, Crustal thickening processes in the Central Andes and the different natures of the Moho-discontinuity: Journal of South American Earth Sciences, v. 12, p. 201–220, doi: 10.1016/S0895-9811(99)00014-0.

Gioncada, A., Hauser, N., Matteini, M., Mazzuoli, R., and Omarini, R., 2006, Mingling and mixing features in basaltic andesites of the Eastern Cordillera (Central Andes, 24°S): A petrographic and microanalytical study: Periodico di Mineralogia, v. 76, p. 127–140.

Glazner, A., 1991, Plutonism, oblique subduction and continental growth: An example from the Mesozoic of California: Geology, v. 19, p. 784–786, doi: 10.1130/0091-7613(1991)019<0784:POSACG>2.3.CO;2.

Goddard, P., Willson, J.J., Couch, S., and Viramonte, J., 1999, The evolution of El Quevar volcanic complex,

Salta Province, Argentina: Congreso Geológico Argentino, 14th, v. 2, p. 225–227.

Gubbels, T.L., Isacks, B.L., and Farrar, E., 1993, High-level surfaces, plateau uplift and foreland development, Bolivian Central Andes: Geology, v. 21, p. 695–698, doi: 10.1130/0091-7613(1993)021<0695:HLSPUA>2.3.CO;2.

Gudmundsson, A., 1998, Magma chambers modeled as cavities explain the formation of rift zone central volcanoes and their eruption and intrusion statistics: Journal of Geophysical Research, v. 103, B4, p. 7401–7412, doi: 10.1029/97JB03747.

Guillou, H., Carracedo, J.C., and Day, S., 1998, Dating of the upper Pleistocene–Holocene volcanic activity of La Palma using the Unspiked K-Ar Technique: Journal of Volcanology and Geothermal Research, v. 86, p. 137–149, doi: 10.1016/S0377-0273(98)00074-2.

Haschke, M., and Ben-Avraham, Z., 2005, Adakites from collision-modified lithosphere: Geophysical Research Letters, v. 32, Art. L15302.

Hauser, N., Matteini, M., Omarini, R., Mazzuoli, R., Vezzoli, L., Acocella, V., Uttini, A., Dini, A., and Gioncada, A., 2005, Aligned extrusive andesitic domes in the southern sector of the Late Miocene Diego de Almagro volcanic complex, Salta-Argentina: Evidences for transtensional tectonics in the Eastern Cordillera: Congreso Geológico Argentino, 16th, Simposio Tectonica Andina, v. 2, p. 153–158.

Hautmann, H.J., and Lippolt, H.J., 2000, $^{40}Ar/^{39}Ar$ dating of central European K-Mn oxides, a chronological framework of supergene alteration processes during the Neogene: Chemical Geology, v. 170, p. 37–80, doi: 10.1016/S0009-2541(99)00241-7.

Heit, B., Kaulakov, I., Asch, G., Yuan, X., Kind, R., Alcozer, I., Tawackoli, S., and Wilke, H., 2005, A teleseismic tomographic image of the Central Andes at 21° S: Terra Nostra, v. 1, p. 55.

Hess, J.C., and Lippolt, H.J., 1994, Compilation of K-Ar measurements on HD-B1 standard biotite, *in* Odin, G.S., ed., Phanerozoic Time Scale: Bulletin of Liaison and Information of the IUGS Subcommission on Geochronology, v.12, p. 19–23.

Hilley, G.E., and Strecker, M.R., 2005, Processes of oscillatory basin filling and excavation in a tectonically active orogen: Quebrada del Toro Basin, NW Argentina: Geological Society of America Bulletin, v. 117, p. 887–901, doi: 10.1130/B25602.1.

Hongn, F.D., Tubia, J.M., Aranguren, A., and Mon, R., 2002, La monzodiorita Las Burras: Un pluton miocenico en el batolito de Tastil, Cordillera Oriental Argentina: Congreso Geológico Argentino, 15th, v. 2, p. 128–133.

Hongn, F.D., Tubia, J.M., Aranguren, A., Mon, R., and Vegas, N., 2005, Intrusion del Granito de Tastil en Areniscas Eopaleozoicas (Angosto de la Quesera, Cordillera Oriental, Salta): Congreso Geológico Argentino, 16th, v. 1, p. 509–514.

Horton, B.K., and DeCelles, P.G., 1997, The modern foreland basin system adjacent to the Central Andes: Geology, v. 25, p. 895–898, doi: 10.1130/0091-7613(1997)025<0895:TMFBSA>2.3.CO;2.

Hrouda, F., Táborská, Š., Schulmann, K., Ježel, J., and Dolejš, D., 1999, Magmatic fabric and rheology of comingled magmas in the Nasavrky Plutonic Complex (E Bohemia): Implications for intrusive strain regime and emplacement mechanism: Tectonophysics, v. 307, p. 93–111, doi: 10.1016/S0040-1951(99)00121-3.

Irvine, T.N., and Baragar, W.R.A., 1981, A guide to the chemical classification of the common volcanic rocks: Canadian Journal of Earth Sciences, v. 8, p. 523–548.

Isacks, B.L., 1988, Uplift of the Central Andean plateau and bending of the Bolivian orocline: Journal of Geophysical Research, v. 93, p. 3211–3231, doi: 10.1029/JB093iB04p03211.

Kay, M.S., and Mpodozis, C., 2001, Central Andean ore deposits linked to evolving shallow subduction systems and thickening crust: GSA Today, v. 11, no. 3, p. 4–9, doi: 10.1130/1052-5173(2001)011<0004:CAODLT>2.0.CO;2.

Kay, R.W., and Kay, S.M., 1993, Delamination and delamination magmatism: Tectonophysics, v. 219, p. 177–189, doi: 10.1016/0040-1951(93)90295-U.

Kay, S.M., Coira, B., and Viramonte, J., 1994, Young mafic back arc volcanic rocks as indicators of continental lithospheric delamination beneath Argentine Puna plateau, central Andes: Journal of Geophysical Research, v. 99, p. 24,323–24,339, doi: 10.1029/94JB00896.

Kay, S.M., Mpodozis, C., and Coira, B., 1999, Magmatism, tectonism and mineral deposits of the Central Andes (22°–33°S), *in* Skinner, B.J., ed., Geology and Ore Deposits of the Central Andes: Society of Economic Geology Special Publication 7, p. 27–59.

Kilmurray, J.O., and Igarzabal, A.P., 1971, Petrografia y rasgos geomorficos del batolito granitico de Santa Rosa de Tastil, provincia de Salta, Rep. Argentina: Revista de la Asociation Geologica Argentina, v. 26, p. 417–438.

Krallmann, A., 1994, Petrographische und geochemische Untersuchungen an jungen, basichen Vulkaniten im Bereich des Calama–Olacapato–El Toro lineamentes ostlich der Vulkankette, NW Argentinien: Clausthaler Geowissenschaftliche Dissertationen, v. 45, 150 p.

Le Bas, M.J., Le Maitre, R.W., Streckeisen, A., and Zanettin, B., 1986, A chemical classification of volcanic rocks based on the total alkali-silica diagram: Journal of Petrology, v. 27, p. 745–750.

Lucassen, F., Lewerenz, S., Frantz, G., Viramonte, J., and Mezger, K., 1999, Metamorphism, isotopic ages and composition of lower crustal granulite xenoliths from the Cretaceous Salta Rift, Argentina: Contributions to Mineralogy and Petrology, v. 134, p. 325–341, doi: 10.1007/s004100050488.

Lucassen, F., Becchio, R., Harmon, R., Kasemann, S., Frantz, G., Trumbull, R., Wilke, H.-G., Romer, R.L., and Dulski, P., 2001, Composition and density model of the continental crust at an active continental margin—The Central Andes between 21° and 27°S: Tectonophysics, v. 341, p. 195–223, doi: 10.1016/S0040-1951(01)00188-3.

Lucassen, F., Escayola, M., Frantz, G., Romer, R.L., and Koch, K., 2002, Isotopic composition of the late Mesozoic basic and ultrabasic rocks from the Andes (23–32° S)—Implication for the Andean mantle: Contributions to Mineralogy and Petrology, v. 143, p. 336–349.

Lucassen, F., Frantz, G., Viramonte, J.G., Romer, R.L., Dulski, P., and Lang, A., 2005, The late Cretaceous lithospheric mantle beneath the Central Andes: Evidence from phase equilibria and composition of mantle xenoliths: Lithos, v. 82, p. 379–406, doi: 10.1016/j.lithos.2004.08.002.

Ludwig, K.R., 2003, User's manual for Isoplot/Ex version 3.00, a geochronological toolkit for Microsoft Excel: Berkeley [California] Geochronology Center Special Publication 4, p. 72.

Luhr, J.F., and Carmichael, I.S.E., 1980, The Colima volcanic complex, Mexico. I: Post-caldera andesites from Volcan Colima: Contributions to Mineralogy and Petrology, v. 71, p. 343–372, doi: 10.1007/BF00374707.

Malamud, B.M., Jordan, T.E., Alonso, R.A., Gallardo, E.F., Gonzalez, R.E., and Kelley, S.A., 2002, Pleistocene Lake Lerma, Salta Province, NW-Argentina: Congreso Geológico Argentino, 13th, v. 4, p. 103–114.

Marquillas, R.A., del Papa, C., and Sabino, I.F., 2005, Sedimentary aspects and paleoenvironmental evolution of a rift basin: Salta Group (Cretaceous–Paleogene), northwestern Argentina: International Journal of Earth Sciences, v. 94, p. 94–113, doi: 10.1007/s00531-004-0443-2.

Marre, J., 1986, The structural analysis of granitic rocks: London, North Oxford Academic, 123 p.

Marrett, R., and Emerman, S.H., 1992, The relations between faulting and mafic magmatism in the Altiplano-Puna plateau (central Andes): Earth and Planetary Science Letters, v. 112, p. 53–59, doi: 10.1016/0012-821X(92)-0006-H.

Marrett, R., and Strecker, M.R., 2000, Response of intracontinental deformation in the central Andes to late Cenozoic reorganization of South American Plate motions: Tectonics, v. 19, p. 452–467, doi: 10.1029/1999TC001102.

Marrett, R.A., Allmendinger, R.W., Alonso, R.N., and Drake, R.E., 1994, Late Cenozoic tectonic evolution of the Puna plateau and adjacent foreland, northwestern Argentine Andes: Journal of South American Earth Sciences, v. 7, p. 179–207, doi: 10.1016/0895-9811(94)90007-8.

Matteini, M., Mazzuoli, R., Omarini, R., Cas, R., and Maas, R., 2002a, The geochemical variations of the upper Cenozoic volcanism along the Calama–Olacapato–El Toro transversal fault system in central Andes (~24°S): Petrogenetic and geodynamic implications: Tectonophysics, v. 345, p. 211–227, doi: 10.1016/S0040-1951(01)00214-1.

Matteini, M., Mazzuoli, R., Omarini, R., Cas, R., and Maas, R., 2002b, Geodynamical evolution of the central Andes at 24°S as inferred by magma composition along the Calama–Olacapato–El Toro transversal volcanic belt: Journal of Volcanology and Geothermal Research, v. 118, p. 205–228, doi: 10.1016/S0377-0273(02)00257-3.

Matteini, M., Acocella, V., Vezzoli, L., Dini, A., Gioncada, A., Guillou, H., Mazzuoli, R., Omarini, R., Uttini, A., and Hauser, N., 2005a, Geology and petrology of the Las Burras–Almagro magmatic complex, Salta, Argentina: Congreso Geológico Argentino, 16th, v. 1, p. 479–484.

Matteini, M., Gioncada, A., Mazzuoli, R., Acocella, V., Dini, A., Guillou, H., Omarini, R., Uttini, A., Vezzoli, L., and Hauser, N., 2005b, The magmatism in easternmost sector of Calama–Olacapato–El Toro transversal fault system in Central Andes at 24°S: Geotectonic significance: International Symposium on Andean Geodynamics, 6th, Barcelona, 12–14 September 2005, Extended Abstracts, p. 499–501, Paris, IDR Editions.

McDonough, W.F., and Sun, S.S., 1995, The composition of the Earth: Chemical Geology, v. 120, p. 223–253, doi: 10.1016/0009-2541(94)00140-4.

McQuarrie, N., Horton, B.K., Zandt, G., Beck, S., and DeCelles, P.G., 2005, Lithospheric evolution of the Andean fold–thrust belt, Bolivia, and the origin of the central Andean plateau: Tectonophysics, v. 399, p. 15–37, doi: 10.1016/j.tecto.2004.12.013.

Mon, R., 1999, Cordillera Oriental, *in* Gonzalez Bonorino, G., et al., eds., Geologia del Noroeste Argentino: Relatorio Congreso Geológico Argentino, 14th, p. 426–431.

Muller, J.P., Kley, J., and Jacobshagen, V., 2002, Structure and Cenozoic kinematics of the Eastern Cordillera, Southern Bolivia (21°S): Tectonics, v. 21, p. 1037, doi: 10.1029/2001TC001340.

Odin, G.S., ed., 1982, Numerical Dating in Stratigraphy: Chichester, UK, Wiley, 2 vols., 1094 p.

Omarini, R.H., and Götze, H.J., 1991, Central Andes Transect, Nazca Plate to Chaco Plains, Southwestern Pacific Ocean, Northern Chile and Northern Argentina: Co-published by Inter-Union Commission on the Lithosphere and American Geophysical Union, Pub. 192, 30 p., 2 sheets.

Omarini, R.H., Sureda, R.J., Götze, H.-J., Seilacher, A., and Pfluger, F., 1999, Puncoviscana folded belt in northwestern Argentina: Testimony of Late Proterozoic Rodinia fragmentation and pre-Gondwana collisional episodes: International Journal of Earth Sciences, v. 88, p. 76–97, doi: 10.1007/s005310050247.

Ort, M.H., Coira, B.L., and Mazzoni, M.M., 1996, Generation of a crust-mantle magma mixture: Magma sources and contamination at Cerro Panizos, central Andes: Contributions to Mineralogy and Petrology, v. 123, p. 308–322, doi: 10.1007/s004100050158.

Paterson, S.R., and Vermon, R.H., 1995, Bursting the bubbles of ballooning plutons; a return to nested diapirs emplacement by multiple processes: Geological Society of America Bulletin, v. 107, p. 1356–1380, doi: 10.1130/0016-7606(1995)107<1356:BTBOBP>2.3.CO;2.

Perugini, D., and Poli, G., 2000, Chaotic dynamics and fractals in magmatic interaction processes: A different approach to the interpretation of mafic microgranular enclaves: Earth and Planetary Science Letters, v. 175, p. 93–103, doi: 10.1016/S0012-821X(99)00282-4.

Petrinovic, I.A., Mitjavila, J., Viramonte, J.G., Marti', J., Becchio, R., Arnosio, M., and Colombo, F., 1999, Description geoquimica y geocronologica de secuencias volcanicas neogenas de trasarco en el estremo oriental de la cadena vulcanica transversal del Quevar (Noroeste de Argentina): Acta Geologica Hispanica, v. 34, p. 255–272.

Petrinovic, I.A., Riller, U., and Brod, J.A., 2005, The Negra Muerta Volcanic Complex, southern Central Andes: Geochemical characteristics and magmatic evolution of an episodically active volcanic centre: Journal of Volcanology and Geothermal Research, v. 140, p. 295–320, doi: 10.1016/j.jvolgeores.2004.09.002.

Renne, P.R., Swisher, C.C., Deino, A.L., Karner, D.B., Owens, T.L., and DePaolo, D.J., 1998, Intercalibration

of standards, absolute ages and uncertainties in $^{40}Ar/^{39}Ar$ dating: Chemical Geology, v. 145, p. 117–152, doi: 10.1016/S0009-2541(97)00159-9.

Reynolds, J.H., Galli, C.J., Hernandez, R.M., Idleman, B.D., Kotila, J.M., Hilliard, R.V., and Naeser, C.W., 2000, Middle Miocene tectonic development of the Transition Zone, Salta Province, northwest Argentina: Magnetic stratigraphy from the Metán Subgroup, Sierra de Gonzalez: Geological Society of America Bulletin, v. 112, p. 1736–1751, doi: 10.1130/0016-7606(2000)112<1736:MMTDOT>2.0.CO;2.

Riller, U., and Oncken, O., 2003, Growth of the Central Andean Plateau by tectonic segmentation is controlled by the gradient in crustal shortening: Journal of Geology, v. 111, p. 367–384, doi: 10.1086/373974.

Riller, U., Petrinovic, I.A., Ramelow, J., Strecker, M.R., and Oncken, O., 2001, Late Cenozoic tectonism, collapse caldera and plateau formation in the Central Andes: Earth and Planetary Science Letters, v. 188, p. 299–311, doi: 10.1016/S0012-821X(01)00333-8.

Salfity, J.A., 1985, Lineamentos transversales al rumbo andino en el Noroeste Argentino: Actas Congreso Geológico Cileno, 4th, v. 1, p. 119–137.

Salfity, J.A., Gorustovich, S.A., Moya, M.C., and Amengual, A., 1984, Marco tectonico de la sedimentation y efusividad Cenozoicas en la Puna Argentina: Congreso Geológico Argentino, 9th, v. 1, p. 539–554.

Sanchez, M.C., and Salfity, J.A., 1999, La cuenca cambrica del Grupo Meson en el Noroeste Argentino: Desarrollo estratigrafico y paleogeografico: Acta Geologica Hispanica, v. 34, p. 123–139.

Scaillet, S., and Guillou, H., 2004, A critical evaluation of young (near-zero) K-Ar ages: Earth and Planetary Science Letters, v. 220, p. 265–275, doi: 10.1016/S0012-821X(04)00069-X.

Scheuber, E., and Giese, P., 1999, Architecture of the Central Andes—A compilation of geoscientific data along a transect at 21°S: Journal of South American Earth Sciences, v. 12, p. 103–107, doi: 10.1016/S0895-9811(99)00008-5.

Scheuber, E., and Reutter, K.J., 1992, Magmatic arc tectonics in the central Andes between 21° and 25°S: Tectonophysics, v. 205, p. 127–140, doi: 10.1016/0040-1951(92)90422-3.

Schwab, K., and Schafer, A., 1976, Sedimentation und Tektonik im mittleren Abschnitt des Rio Toro in der Ostkordillere NW-Argentiniens: Geologische Rundschau, v. 65, p. 175–194, doi: 10.1007/BF01808462.

Sillitoe, R., 1977, Permo-Carboniferous, Upper Cretaceous, and Miocene porphyry copper–type mineralization in the Argentinian Andes: Economic Geology and the Bulletin of the Society of Economic Geologists, v. 72, p. 99–109.

Skilling, I.P., White, J.D.L., and McPhie, J., 2002, Peperite: A review of magma-sediment mingling: Journal of Volcanology and Geothermal Research, v. 114, p. 1–17, doi: 10.1016/S0377-0273(01)00278-5.

Snyder, D., 2000, Thermal effects of the intrusion of basaltic magma into a more silicic magma chamber and implications for eruption triggering: Earth and Planetary Science Letters, v. 175, p. 257–273, doi: 10.1016/S0012-821X(99)00301-5.

Spell, T.L., and McDougall, I., 2003, Characterization and calibration of $^{40}Ar/^{39}Ar$ dating standards: Chemical Geology, v. 198, p. 189–211, doi: 10.1016/S0009-2541(03)00005-6.

Spera, F.J., and Bohrson, W.A., 2001, Energy-constrained open-system magmatic processes I: General model and energy-constrained assimilation and fractional crystallization (EC-AFC) formulation: Journal of Petrology, v. 42, p. 999–1018, doi: 10.1093/petrology/42.5.999.

Stern, R.J., 2002, Subduction zones: Reviews of Geophysics, v. 40, p. 1–38.

Streckeisen, A., and Le Maitre, R.W., 1979, A chemical approximation to the modal QAPF classification of igneous rocks: Neues Jahrbuch für Mineralogie-Abhandlungen, v. 136, p. 169–206.

Swenson, J.L., Beck, S.L., and Zandt, G., 2000, Crustal structure of the Altiplano from broadband regional waveform modeling: Implications for the composition of thick continental crust: Journal of Geophysical Research, v. 105, p. 607–621, doi: 10.1029/1999JB900327.

Sylvester, A.G., 1988, Strike-slip faults: Geological Society of America Bulletin, v. 100, p. 1666–1703, doi: 10.1130/0016-7606(1988)100<1666:SSF>2.3.CO;2.

Thorpe, R.S., O'Callaghan, L.J., and Francis, P.W., 1984, Relative roles of source composition, fractional crystallization and crustal contamination in the petrogenesis of Andean volcanic rocks: Philosophical Transactions of the Royal Society of London—A, v. 310, p. 675–692, doi: 10.1098/rsta.1984.0014.

Tikoff, B., and de Saint Blanquat, M., 1997, Transpressional shearing and strike-slip partitioning in the Late Cretaceous Sierra Nevada magmatic arc, California: Tectonics, v. 16, p. 442–459, doi: 10.1029/97TC00720.

Tikoff, B., and Teyssier, C., 1992, Crustal-scale, en echelon "P shear" tensional bridges: A possible solution to the batholithic room problem: Geology, v. 20, p. 927–930, doi: 10.1130/0091-7613(1992)020<0927:CSEEPS>2.3.CO;2.

Tobisch, O., and Cruden, A.R., 1995, Fracture controlled magma conduits in an obliquely convergent continental magmatic arc: Geology, v. 23, p. 941–944, doi: 10.1130/0091-7613(1995)023<0941:FCMCIA>2.3.CO;2.

Trumbull, R.B., Wittenbrink, R., Hahne, K., Emerman, R., Büsch, W., Gerstenberger, H., and Siebel, W., 1999, Evidence for Late Miocene to Recent contamination of arc andesites by crustal melts in the Chilean Andes (25–26°S) and its geodynamic implications: Journal of South American Earth Sciences, v. 12, p. 135–155, doi: 10.1016/S0895-9811(99)00011-5.

Tubia, J.M., Aranguren, A., Hongn, F., and Mon, R., 1999, Datos preliminares sobre la estructura y emplazamiento del Batolito de Santa Rosa de Tastil, Salta: Congreso Geológico Argentino, 14th, v. 1, p. 123–125.

Vaggelli, G., Olmi, F., and Conticelli, S., 1999, Quantitative electron microprobe analysis of reference silicate mineral and glass samples: Acta Vulcanologica, v. 11, p. 297–304.

White, J.L.D., McPhie, J., and Skilling, I., 2000, Peperite: A useful genetic term: Bulletin of Volcanology, v. 62, p. 65–66, doi: 10.1007/s004450050293.

Wood, D.A., Joron, J.L., and Treuil, M., 1979, A re-appraisal of the use of trace elements to classify and discriminate between magma series erupted in different tectonic settings: Earth and Planetary Science Letters, v. 45, p. 326–336, doi: 10.1016/0012-821X(79)90133-X.

Yuan, X., Sobolev, S.V., and Kind, R., 2002, Moho topography in the Central Andes and its geodynamic implication: Earth and Planetary Science Letters, v. 199, p. 389–402, doi: 10.1016/S0012-821X(02)00589-7.

Zandt, G., Velasco, A.A., and Beck, S.L., 1994, Composition and thickness of the southern Altiplano crust, Bolivia: Geology, v. 22, p. 1003–1006, doi: 10.1130/0091-7613(1994)022<1003:CATOTS>2.3.CO;2.

Manuscript Received 7 September 2006
Revised Manuscript Received 27 February 2007
Manuscript Accepted 27 February 2007

Printed in the USA